

Author response

We thank the Co-editor for the review. The updated manuscript has been carefully revised by several people and we used the free version of the 'grammarly' software to correct any mistakes in the grammar.

Please note that we also changed the order of the Figures in order to make the structure of the updated manuscript more logical. Previous Figure 8 is now Figure 4.

Ground-based observation of clusters and nucleation mode particles in the Amazon

Daniela Wimmer¹, Stephany Buenrostro Mazon¹, Hanna Elina Manninen^{1,2}, Juha Kangasluoma¹, Alessandro Franchin^{1,3,4}, Tuomo Nieminen^{1,5}, John Backman⁶, Jian Wang⁸, Chongai Kuang⁸, Radovan Krejci⁷, Joel Brito^{9,10}, Fernando Goncalves Morais⁹, Scot Turnbull Martin¹¹, Paulo Artaxo⁹, Markku Kulmala¹, Veli-Matti Kerminen¹ and Tuukka Petäjä¹

¹Department of Physics, University of Helsinki, Gustaf Hallströmin katu 2a, 00560, Helsinki, Finland

²European Organization for Nuclear Research (CERN), 1211 Geneva, Switzerland

³NOAA Earth System Research Laboratory (ESRL), Chemical Sciences Division, Boulder, CO, USA

⁴Cooperative Institute for Research in Environmental Sciences, University of Colorado Boulder, Boulder, CO, USA

⁵Department of Applied Physics, University of Eastern Finland, Post Office Box 1627, 70211 Kuopio, Finland

⁶Finnish Meteorological Institute, Atmospheric composition research, Erik Palménin aukio 1, 00560, Helsinki, Finland

⁷Stockholm University, Department of Environmental Science and Analytical Chemistry (ACES), 106 91 Stockholm, Sweden

⁸Environmental and Climate Sciences Department, Brookhaven National Laboratory, Upton, New York, USA

⁹Institute of Physics, University of São Paulo, de Física, Universidade de São Paulo, Rua do Matao 1371, CEP 05508-090, São Paulo, Brazil

¹⁰Laboratory for Meteorological Physics (LaMP), Université Clermont Auvergne, F-63000 Clermont-Ferrand, France

¹¹School of Engineering and Applied Sciences, Harvard University Cambridge, Massachusetts 02138, United States of America

Correspondence to: Daniela Wimmer (daniela.wimmer@helsinki.fi)

Keywords: atmospheric ions, particle formation, rainforest, high-frequency rainfall

41 Abstract

42

43 We investigated atmospheric new particle formation (NPF) in the Amazon rainforest using direct
44 measurement methods. To our knowledge this is the first direct observation of NPF events in the
45 Amazon region. However, previous observations elsewhere in Brazil showed the occurrence of
46 nucleation mode particles. Our measurements covered two field sites and both wet and dry season.
47 We measured the variability of air ion concentrations (0.8 – 12 nm) with an ion spectrometer
48 between September 2011 and January 2014 at a rainforest site (T0t). Between February and
49 October 2014, the same measurements were performed at a grassland pasture site (T3) as part of
50 the GoAmazon 2014/5 Experiment, with two intensive operating periods (IOP1 and IOP2 during the
51 wet and the dry season respectively). The GoAmazon 2014/5 Experiment was designed to study the
52 influence of anthropogenic emissions on the changing climate in the Amazon region. The
53 experiment included basic aerosol and trace gas measurements at the ground, remote sensing
54 instrumentation and two aircraft-based measurements.

55 The results presented in this work are from measurements performed at ground level at both sites.
56 The site inside the rainforest (T0t) is located 60 km NNW of Manaus and influenced by pollution
57 about once per week. The pasture (T3) site is located 70 km downwind from Manaus and influenced
58 by the Manaus pollution plume typically once per day or every second day, especially in the
59 afternoon. No new particle formation (NPF) events were observed inside the rainforest (site T0t) at
60 ground level during the measurement period. However, rain-induced ion and particle bursts
61 (hereafter, “rain-events”) occurred frequently (643/1031 days) at both sites during the wet and dry
62 season, being most frequently during the wet season. During the rain-events, the ion concentrations
63 in three size ranges (0.8-2 nm, 2-4 nm and 4-12 nm) increased up to about 10^4 - 10^5 cm⁻³. This effect
64 was most pronounced in the intermediate and large size ranges, where the background ion
65 concentrations were about 10 – 15 cm⁻³, as compared with 700 cm⁻³ for the cluster ion background.
66 We observed 8 NPF events at the pasture site during the wet season. We calculated the growth
67 rates and formation rates of neutral particles and ions for the size ranges 2-3 nm and 3-7 nm using
68 the ion spectrometer data. The observed median growth rates were 0.8 nm h⁻¹ and 1.6 nm h⁻¹ for 2-
69 3 nm-sized ions and particles, respectively, with larger growth rates (13.3 nm h⁻¹ and 7.9 nm h⁻¹) in
70 the 3-7 nm size range. The measured nucleation rates were of the order of 0.2 cm⁻³ s⁻¹ for particles
71 and $4\text{--}9 \times 10^{-3}$ cm⁻³ s⁻¹ for ions. There was no clear difference in the sulfuric acid concentrations
72 between the NPF event days and non-event days ($\sim 9 \times 10^5$ cm⁻³). The two major differences between
73 the NPF days and non-event days were a factor of 1.8 lower condensation sink on NPF event days
74 (1.8×10^{-3} s⁻¹) compared to non-events (3.2×10^{-3} s⁻¹) and different air mass origins.

75 To our knowledge, this is the first time that results from ground-based sub-3 nm aerosol particle
76 measurements have been obtained from the Amazon rainforest.

77 1 Introduction

78

Globally, atmospheric new particle formation (NPF) and growth has been estimated to account for a major, if not dominant, fraction of cloud condensation nuclei (Merikanto et al. 2009, Wang and Penner, 2009, Yu and Luo, 2009, Dunne et al., 2016, Kulmala et al., 2016). The formation of atmospheric nanoparticles is a multi-stage process, in which stable clusters form from gas phase precursors, followed by the activation of these clusters and their further growth (Kulmala et al. 2014). Although atmospheric NPF is occurring frequently in many environments (e.g. Kulmala et al. 2004, Manninen et al. 2010), the Amazon basin is one of the locations where the initial steps of the formation of nanoparticles have not been previously observed from ground-based measurements (Martin et al, 2010a).

In the Amazon basin, emissions and oxidation of volatile organic compounds (e.g. Lelieveld et al. 2008), aerosol activation to cloud droplets, and eventually rain formation, are tightly connected with synoptic processes, such as deep convection (e.g. Lelieveld et al. 2008, Wang et al., 2016). Aerosol concentrations in the Amazonian atmosphere are rapidly changing as a result of deforestation and the associated biomass burning and economic development in the Amazon region (Martin et al. 2016, Artaxo et al., 2013). The Manaus metropolis (population 2 million) is the capital of the state of Amazonia, Brazil, surrounded by the largest rainforest on Earth (Martin et al, 2017), as shown in Fig. 1.

The measurements discussed in this paper took place at two different locations in the Amazon rainforest: a pasture site 70 km downwind from Manaus (T3; Martin et al., 2016); and a site within the rainforest, mostly unaffected by Manaus pollution (T0t; Martin et al., 2010b). The sites are described in more detail in section 2.1. Depending on the wind direction, these sites can represent (i) one of the most anthropogenically undisturbed continental locations on Earth, or (ii) a location affected by both polluted and clean air masses (Martin et al., 2016). The complexity of the mixture of trace gases and aerosol population make the Amazon rainforest an interesting place to study. During most of the wet season, the Amazon basin is one of the cleanest continental regions on Earth (Andreae, 2007; Martin et al., 2010a, Artaxo et al., 2013, Andreae et al., 2015). During the dry season, the Amazon basin is highly influenced by anthropogenic emissions mostly from biomass burning. Additionally, our study region experiences frequent high-intensity precipitation episodes.

The primary goal of this paper was to investigate the characteristics of the wet and the dry season at different sampling locations and the occurrence of new particle formation (NPF) and growth in the Amazon region, and to quantify the role of ions and aerosol particles in this process.

2 Methods

The measurements inside the rainforest at site T0t were performed over 3 years from September 2011 to January 2014. The second measurement site (T3) was part of the Green Ocean Amazon (GoAmazon2014/5) Experiment (Martin et al., 2016). The GoAmazon2014/5 Experiment operated from January 1, 2014 to December 31, 2015. The experiment included two intensive operation periods (IOP1 and IOP2). IOP1 extended from February 1, 2014 to March 31, 2014 and IOP2 from

119 August 15, 2014 to October 15, 2014 (Martin et al., 2016). The ion spectrometer measurements
120 were conducted from January 28 to October 13, 2014. Figure 1 shows the locations of both
121 measurement sites. Table 1 shows an overview over the available dataset presented in this study.

122 2.1. Measurement sites

123

124 2.1.1 Measurement site inside the rainforest

125

126 The T0t ecological reserve (Martin et al, 2010b) is a terrestrial ecosystem science measurement site
127 located 70 km NNW of the Manaus metropolis in the central region of Brazil (2.609°S, 60.2092°W).
128 Two major rivers, the Solimoes and the Rio Negro converge in Manaus to become the Amazon river.
129 The city of Manaus is the capital of the state of Amazonia, Brazil, with more than 2 million
130 inhabitants (IBGE, 2015). It is the seventh biggest city in Brazil and is surrounded by forest for 1500
131 km in all directions (Martin et al., 2016).

132

133 T0t is surrounded by a dense rainforest. The rainforest canopy is homogeneous with an average
134 height of 30 m. T0t is influenced by anthropogenic pollution about once per week (Martin et al.,
135 2010b supplementary material, Thalmann et al, 2017, de Sa et al, 2017). Otherwise, the location of
136 the T0t site allows the characterization of an almost completely undisturbed environment (Martin
137 et al, 2016).

138

139 2.1.2 Open pasture measurement site

140

141 The open pasture site, T3, is influenced by the Manaus pollution plume typically once per day or
142 every second day, especially in the afternoon (Martin et al., 2010b supplementary material,
143 Thalmann et al, 2017, de Sa et al, 2017). A Mobile Facility from the Atmospheric Radiation
144 Measurement (ARM) Program (Mather et al., 2014) of the United States Department of Energy was
145 deployed at the T3 site close to Manacapuru, about 70 km downwind of the city of Manaus
146 (3.2133°S, 60.5987°W), and included an ARM Mobile Aerosol Observing System (MAOS). The site
147 also hosted numerous instrument systems from other GoAmazon2014/5 participants (Martin et al.,
148 2016).

149

150 2.2 Instrumentation

151

152 2.2.1 Neutral cluster and Air Ion Spectrometer (NAIS)

153

154 A Neutral cluster and Air Ion Spectrometer (NAIS; Manninen et al., 2016) was used to determine the
155 early stages of atmospheric nucleation and subsequent growth. The NAIS measures the mobility
156 distributions in the range $3.2 - 0.0013 \text{ cm}^2 \text{ V}^{-1} \text{ s}^{-1}$, which corresponds to a mobility equivalent
157 diameter range of 0.8 – 42 nm. The ion and neutral particle size distributions are measured in three
158 different stages: ion, particle, and offset. The NAIS consists of two parallel cylindrical DMAs

(Differential Mobility Analyzers), one for classifying negative ions and the other for positive ions. In the ion mode, the corona chargers and the electrostatic filters are switched off to allow only naturally-charged ions to enter the DMA. During the particle mode, the particles are charged by a corona charger in order to be detected by the DMA. The inlet flow into the NAIS is 60 liters per minute (Lpm), whereas the sample and the sheath flows of the DMAs are 30 and 60 Lpm, respectively. The NAIS time resolution was set to 5 min, which includes a full measurement cycle of negative ions, positive ions and total particles. The NAIS instrument and calibration are described in more details in Asmi et al. (2009), Wagner et al. (2016) and Manninen et al. (2016). The NAIS measurement accuracy was estimated to be 10 - 30%, which was mainly due to flow rate uncertainties (Manninen et al., 2016; Wagner et al., 2016). The electrometers measure a current which can be transformed into particle/ion concentrations. If the measured currents are low, the noise can be quite high and can result in negative concentration values. The environmental conditions in the Amazon are very challenging for NAIS measurements, especially the high relative humidity (RH). To reduce the NAIS sampling RH, an electric heater was installed at the inlet to heat the sampling air to 60° C in order to evaporate some water before entering the instrument.

The NAIS was placed inside a hut at the T0t site, sampling at 2 m above the ground level. In January 2014, the NAIS was moved to the T3 site where it was placed outside under a roof. The sampling setup was the same at both sites. In total 736 days of neutral particle data and 718 days of ion data were taken at both sites together (see Table 1).

2.2.2 Particle Size Magnifier (PSM)

A Particle Size Magnifier (PSM; Airmodus A09; Vanhanen et al., 2011) was used to determine aerosol particle concentrations at sizes below 3 nm. The PSM is a mixing-type condensation particle counter (CPC), in which the aerosol is turbulently mixed with air saturated with diethylene glycol (DEG). DEG only grows the particles to about 90 nm, so the PSM system consists of a second stage, where the particles are grown to optically-detectable sizes. The 50% activation diameter of the instrument can be varied across a size range of 1–4 nm in a mobility diameter (Vanhanen et al., 2011) by changing the mixing ratio between the saturator and the sample flow. At GoAmazon2014/5, the PSM was used in a scanning mode in which the saturator flow is continuously changing, altering the cut-off diameters between 1 and 4 nm. One scan takes 4 minutes and the system was set up to do one upscan, followed by a downscan. Due to the challenging measurement conditions, the size-resolved data was not used in this analysis.

Prior to the deployment during the GoAmazon2014/5 campaign, the PSM system was equipped with an inlet system specifically designed to decrease the relative humidity of the sample without disturbing the sample itself and to maintain high flow rates to minimize diffusion losses. The inlet system comprises a core sampling probe combined with a sintered tube. The core sampling probe consists of two cylindrical tubes with different outer diameters (10 mm and 6 mm). The larger diameter of the outer tube allows a total laminar flow rate of up to 10 Lpm, to minimize diffusional

losses. The inner tube is directly attached to the PSM with an airflow of 2.5 Lpm. The excess airflow is discarded into an exhaust line (Kangasluoma et al., 2016). Downstream of the core sampling line there is a sintered tube where dry, pressurized air is introduced. The water molecules in the sample flow are pushed towards the outer walls of the sintered material by diffusion, drying the airflow. Laboratory studies have shown that RH can drastically affect the PSM counting efficiency (higher sensitivity at smaller sizes at higher RH; Kangasluoma et al, 2013, Iida et al, 2009).

Since the aerosol in Brazil was expected to be composed of mostly organic species, the PSM with the inlet was calibrated using limonene and its oxidation products (Kangasluoma et al., 2014) as a test aerosol. The resulting lowest PSM cut-off diameter was 1.5 nm (± 0.3 nm), where the uncertainty was estimated as a combination of the calibration uncertainty and the influence of the ambient RH on the PSM cut-off diameter. In total, 38 days of data obtained during the dry season were used.

2.2.3. Supporting instrumentation at both sites

At T0t, the submicron aerosol number size distributions and total particle number concentrations were monitored with a DMPS system (Aalto et al., 2001) and a CPC. The CPC time resolution was 1 minute, with a 50% cut-off size of about 6 nm. The DMPS measured number size distributions over the mobility diameter range of 6 – 800 nm (Backman et al., 2012), and a complete size distribution was obtained every 10 minutes. During the 10-minute measurement cycle, size-segregated aerosols were measured for 8 minutes, followed by 2 minutes of total particle number concentration measurements, using a bypass valve. The transmission at 4 nm of the inlet used the AMAZE-08 (Martin et al., 2010b) experiment was 50%. The diffusion losses increase exponentially with a decreasing particle size. For the measurements reported here, a similar setup with a 60 m sampling line was used. The DMPS data should be used in a qualitative rather than quantitative manner as the losses due to diffusion in the sampling line are not precisely known and therefore not considered. In addition to the ion spectrometer measurements, the measurement hut hosted an automated weather system (Vaisala; WXT-520) for acquiring meteorological parameters.

The auxiliary data from the T3 site, presented in this manuscript includes measurements from an ultrafine CPC (TSI Inc; 3010), with a 50% activation diameter of 10 nm and an SMPS with a lower cut-off of 20 nm. The meteorological data were also retrieved from an automated weather station (Vaisala; WXT-520). Those datasets are available at the ARM data browser.

2.3 Measurement periods: wet and dry season

The differences in the tropical seasons present contrasting environmental conditions (Martin et al., 2016, Artaxo et al., 2013). In our manuscript, we follow Artaxo et al. (2013) and define the wet season in the Amazon from January to June, and the dry season from July to December.

239 The most dominant anthropogenic influence in the Amazon region is dictated by biomass burning
240 emissions, which are strongest during the dry season. The most intense biomass burning and
241 atmospheric perturbations take place at the southern and eastern edges of the forest (Brito et al.,
242 2014), however, their transport impacts the whole basin. During the wet season, Manaus emissions
243 are the main anthropogenic influence on the aerosol population in the Amazon region (Andreae,
244 2007; Martin et al., 2010a). During the dry season, the wet deposition decreases whereas the
245 condensation sink increases. That leads to an overall increase in aerosol concentration in the
246 accumulation mode of about one order of magnitude even in remote areas (Artaxo et al., 2013).

247
248 The planetary boundary layer development displays a strong diel behavior, with a stable nocturnal
249 layer and strong vertical mixing during the daytime. The vertical transport is enhanced in strong
250 convective situations when particles are lofted and entrained into the free troposphere. The stable
251 nocturnal layer, on the other hand, traps the emissions near the surface; the impact can be more
252 pronounced during the dry season as biomass burning usually starts at midday and continues into
253 evening hours (Martin et al, 2010a). The boundary layer development is also different for the two
254 different measurement sites, as the boundary layer develops more rapidly over the pasture area,
255 with more efficient vertical mixing compared to the site enclosed by the rainforest.

256 2.4 Data analysis

257
258 All the available data from the NAIS were cleaned for a potential instrumental noise. The cleaning
259 process was done visually using the particle and ion size distributions as surface plots. The non-
260 reliable data were removed based on the guidelines introduced by Manninen et al. (2010). The NAIS
261 data turned out to be unreliable during the measurements presented here mostly in the size range
262 above 15 nm. Therefore, we decided to show data for the sizes up to 12 nm only in our analysis. We
263 divided the measured ion and neutral particle concentrations into three sub size-ranges: cluster
264 size-range (0.8 - 2 nm), intermediate size-range (2 - 4 nm), and large size-range (4 - 12 nm). Defining
265 the lower and upper limits of the intermediate ion size range varies in the scientific literature (see
266 Hirsikko et al., 2011 and references therein). The definition of using 2-4 nm as intermediate size-
267 range allows for differentiating between new particle formation events and non-events when using
268 ion measurements (Leino et al., 2016).

269
270 We observed an increase in the concentrations of the cluster ions in the NAIS starting from October
271 7, 2013 to January 21, 2014. By investigating the raw data files, this drift was observed to be due to
272 too low currents in the sheath air filters. The sheath air filters are electrical filters, using corona
273 needles to neutralize all the remaining ions, which leads to an over-estimation of ion concentrations.
274 A correction factor of 1.8 was applied to account for this problem in the 4 smallest size channels of
275 the NAIS (0.8-1.25 nm) for the data taken at the T0t site after the drift was observed. This increased
276 level in the positive polarity of the natural ions continued when the NAIS was re-deployed at the T3
277 site. The cause was the same (too low a current in the sheath air filters). We consider the positive
278 polarity of the natural charged ions in the NAIS at the T3 site unreliable, therefore the data,

279 regarding the absolute concentrations, using the positive channel for the T3 site is not shown in this
280 study. Additionally, the ion data from September 9-26, 2014 at the T3 site was considered unreliable
281 and was also excluded from our analysis.

282
283 Rain-induced ion events were selected as the times when an ion burst coincided with the onset of
284 precipitation. The median and the maximum (99th percentile) ion concentrations were calculated
285 during the periods when the rain intensity was $>0 \text{ mm h}^{-1}$. In case of more than one rain-event per
286 day, two separate rain-events were classified as such, if the start of the second one occurred more
287 than an hour after the end of the first one. Any fluctuations in the rain intensity for a time period
288 shorter than 1 hour were considered to be part of a single rain-event. We classified 962 rain-events
289 at the T0t site and 221 rain-events at the T3 site.

290 The new particle formation event analysis from the ion spectrometer data, including the event
291 classification and formation and growth rate calculations, followed the already well-defined
292 guidelines (Kulmala et al., 2012). In the data analysis, the first step was to classify all available days
293 into NPF event and non-event days according to methods introduced earlier by Hirsikko et al. (2007)
294 and Manninen et al. (2010). The days that do not fulfill the criteria of an event or non-event day,
295 are categorized as undefined days. However, no days were classified as undefined in this study.

296
297 The classification was performed manually through a visual inspection of daily contour plots of
298 particle number size distributions. The second step in the analysis was to define the characteristics
299 related to each NPF event, such as the particle growth rate (GR) and formation rate (J). The GRs
300 were calculated for two different size bins (2-3 nm and 3-7 nm in particle diameter) using both ion
301 and neutral particle data from the NAIS. The particle growth rate was determined by finding the
302 times at which the maximum concentrations of ions/particles in each of these size ranges occurred.
303 A fit between the points was then applied to resolve the growth rates. The particle formation rate
304 was determined for the lower end of each size bin (2 and 3 nm) by taking the particle growth rate,
305 condensation sink and coagulation sink into account.

306

307 3 Results

308

309 All the times mentioned below are local Manaus time (LT), which is Coordinated Universal Time
310 (UTC) – 4 h.

311 3.1 Number concentrations of ions and particles at the two sites

312

313 An overview of the observed number concentrations of ions and particles together with the
314 meteorological conditions at the two measurement sites is presented in Table 2.

315

316 When comparing the two measurement sites, the most apparent differences are: (i) the almost
317 factor of 3 lower intermediate negative ion concentrations at the T3 site compared to the T0t site
318 (6 cm^{-3} and 5 cm^{-3} during the wet and dry season, respectively, at T3; 17 cm^{-3} during both wet and

dry season at T0t). This difference is likely to be caused by the enhanced formation of negative ions by the precipitation. (ii) By contrast, the large-sized ion concentrations were about a factor of 2 higher at the T3 site compared to the T0t site (20 cm^{-3} and 12 cm^{-3} during the wet and dry season, respectively, at T3; 8 cm^{-3} during both wet and dry season at T0t). (iii) Also, the intermediate and large-sized neutral particles were by about a factor of 3 higher at the T3 compared to the T0t site. These enhanced concentrations were probably due to a combination of stronger mixing of the boundary layer and the occurrence of NPF events at the T3 site.

The environmental variables were relatively similar at the two measurement sites, with higher average temperatures and lower average RH at the T3 site compared to the T0t site. The wind directions at both sites varied from the wet to the dry season. At T3, the air masses arrived, on average, from 115° N during the wet season and from 95° N during the dry season. At T0t, the average wind direction changed from 94° during the wet season to 105° N throughout the dry season (see Table 2).

3.1.1 Inside rainforest site (T0t)

At the T0t site, the negative cluster ion concentrations were very comparable during the wet (856 cm^{-3}) and the dry season (952 cm^{-3}). The positive cluster ion concentrations were by about a factor of 1.7 lower throughout both seasons compared to the negative ions (549 cm^{-3} (wet) and 537 cm^{-3} (dry)). These values are comparable to those observed in several other locations (eg. urban Paris, Dos Santos et al. 2015; coastal Mace Head, Vana et al. 2008 and Finokalia, Kalvitis et al. 2012; Puy de Dome, Rose et al. 2016).

The ion concentrations in the intermediate size range (2-4 nm) were a factor of 2 higher in the positive polarity compared to the negative polarity both in the wet and in the dry season (17 cm^{-3} (-) and 34 cm^{-3} (+) during the wet season; 17 cm^{-3} (-) and 34 cm^{-3} (+) during the dry season). We observed the same concentrations in the large size range on the other hand in both polarities and both seasons (8 cm^{-3}). The neutral particle concentrations were higher in the intermediate (2-4 nm) size range compared to the large (4-12 nm) size range, being very similar in the wet and dry season. The characteristics of the wet and the dry season in the Amazon (Rissler et al. 2006, Martin et al. 2010a) can be observed in the concentrations of the negative ions as shown in Figure 2. The negative ion concentrations were decreasing from April to September and increasing between September and February. Most likely, the local biomass burning during the dry season increased the ion concentrations. During the wet season, the ion concentrations decreased most likely due to wet deposition and reduced source strengths.

We observed a similar diel pattern for both the wet and the dry season for the neutral particles as shown in Figure 3. The concentrations in both size ranges increase at around 06:00 – 09:00 during the wet season. This effect was less pronounced in the dry season. A clear decrease in neutral particle concentrations during evening times (after 17:00) can be observed.

3.1.2. Pasture site (T3)

As shown in Table 2, cluster ion concentrations at the T3 site were typically higher during the wet season (1300 cm^{-3}) than the dry season (890 cm^{-3}). Similar, high ion concentrations were reported in an Australian rainforest in Tumbarumba (Suni et al. 2008) and in a wetland site in Abisko (Svennigsson et al., 2008). Those experiments showed concentrations of ~ 2400 (1700) cm^{-3} for negative (positive) ions. The median negative ion concentrations in the intermediate and large size ranges ($2 - 4\text{ nm}$ and $4 - 12\text{ nm}$) were very similar during the wet season (6 cm^{-3} , 20 cm^{-3}) and the dry season (5 cm^{-3} , 12 cm^{-3}). The neutral particle concentrations were also very similar in both seasons at the T3 site. The median total concentrations measured by the ultrafine MAOS CPC ($>10\text{ nm}$) were observed to be more than a factor of 2 higher in the dry season than in the wet season (928 cm^{-3} versus 2000 cm^{-3}). This difference is most likely due to the enhanced biomass burning during the dry season. The average temperatures and the average relative humidity were very similar in both seasons.

The PSM measurements were performed during the dry season only. In total, 38 days of PSM data were included in this study and the results are shown in Figure 4. The PSM was used in scanning mode but, due to the challenging environmental conditions, only data measured at the highest supersaturation (total particle concentration at $>1.5\text{ nm}$) is shown. The PSM data showed a similar diel pattern as the cluster ion concentrations measured by the NAIS (see Fig. 9), with higher median concentrations observed during the early morning (03:00-06:00), a dip in concentrations during the early afternoon (12:00-15:00), and then elevated median concentrations again in the evening (18:00-24:00). This could be explained by the Carnegie curve (Harrison, R. G. and Carslaw, K. S., 2003), which manifests as a diel variation in the ionospheric potential.

3.2 Rain-induced ion formation events

While no NPF events were observed within the rainforest at site T0t, rain-induced ion burst events (hereafter, rain-events) were common and observed during 264 out of the 384 measurement days. Since multiple rain episodes could occur in a single day, each rain-event was investigated separately, giving a total of 962 rain-events at T0t site and 221 at the T3 site.

Figure 5 shows an example of multiple rain-events that took place during January 24, 2013 (wet season). The negative ion concentrations in the cluster size range of $0.8 - 2\text{ nm}$ increased during the precipitation from about 1000 cm^{-3} to 1500 cm^{-3} . The positive cluster ion concentrations on the other hand decreased during the precipitation episode from 1000 cm^{-3} to about 500 cm^{-3} . The intermediate ($2 - 4\text{ nm}$) ion concentrations showed an increase in both polarities, although the buildup was more pronounced for the negative intermediate-sized ions. In the intermediate size range, the concentrations of negative ions reached up to 3000 cm^{-3} , while during the same

precipitation event, the positive intermediate ion concentrations only rose to 200 cm^{-3} . A similar feature for 2-8 nm-sized negative ions during rain-events has also been reported for an Australian rainforest (Suni et al. 2008). In that study, the positive ion concentrations increased only in the 3-7 nm size range and decreased in the 1-3 nm size range during the precipitation episodes. These rain-induced ion bursts are thought to be a result of a balloelectric effect, in which splashing water produces intermediate ions, such that the negative ions are smaller in size than the positive ions (Horrak et al., 2005, Hirsikko et al., 2007, Tammet et al., 2009).

The duration of the 962 rain-events in our study varied from a couple of minutes to 22 hours, with over half of the rain-events lasting for two hours or less. The statistics of the rain-event frequency from the T0t measurement site are shown in Figure 6. The bars show the mean number of days with and without rain and the black line shows the median total average precipitation per month. Figure 6 shows that rain-events occurred in both seasons. However, the number of days without rain increased during the dry season (July to December).

Figure 7 shows the correlation between the maximum negative ion concentration and the median rain intensity during each rain-event. While no clear connection between these two quantities was found, two specific features are apparent: at the site within the canopy (T0t), the highest cluster and intermediate ion concentrations occurred almost entirely in correlation with rather strong rain intensities, whereas at the pasture site (T3) almost no increase in negative ion concentrations in any size range during precipitation periods could be observed.

The rain-events were also evident in the total particle concentration measured by the NAIS, as depicted in Figure 8. In this example, the rain intensity peaks twice, about 40 mm h^{-1} at ~09:00 followed by a second peak of 10 mm h^{-1} at ~11:00. The ion and particle concentrations measured by the NAIS increased and decreased almost simultaneously with the increase and decrease of the precipitation rate. Additionally, the DMPS data showed an appearance of nucleation mode particles between 6 and 10 nm, also following the onset of the rain. Please note, that the DMPS was sampling at a height of 60 m, which is well above the rainforest canopy. The concentration of 6-10 nm particles increased by a factor of 4 during the rain-event, as compared to a background concentration of 5 cm^{-3} in the absence of precipitation. The 10-20 nm particle concentrations first showed a drop, followed by an increase up to $\sim 35 \text{ cm}^{-3}$. The maximum concentrations of the 10 – 20 nm particles appeared about 4 hours after the short-term increase of the 6-10 nm particles.

The appearance of 6-10 nm particles and their peak concentration could present a similar scenario as observed in Wang et al (2016). They reported a production of small aerosol particles as a result of new particle formation in cloud outflow regions, with further transport into the boundary layer due to strong convection during precipitation events in the Amazon. Wang et al. (2016) noted that the $<20 \text{ nm}$ particle concentrations decreased very rapidly. We suggest the process that we observe is a local one because the production of ions was observed to only last for the duration of the precipitation.

3.3 New particle formation events at T3

We observed no NPF events during the dry season. During the wet season, on 9% of the days, we did observe NPF events. A similar event frequency has been observed in the Finnish boreal forest environment during the autumn as an example (Kontkanen et al., 2017). An earlier study by Backman et al. (2012) showed that in the metropolitan area of São Paulo (population 20 million), Brazil, NPF events occurred on 11% of the days. Zhou et al. (2002) observed an ultrafine particle mode in central Amazonia on 18% of the measurement days.

We selected all eight NPF event days to characterize the behavior of ions and aerosol particles during the bursts of particle formation. A comparison of the diel cycle for particles and ions between NPF and non-event days is shown in Figure 9. The cluster ions showed a clear diel cycle with higher concentrations in the morning and evening for both NPF and non-event days. An increase in the concentrations of intermediate and large ions (2-4 nm and 4-12 nm) occurred during NPF event days, which was due to the growth of the ions from the cluster ion size range (0.8-2 nm) to larger sizes. The intermediate neutral particle concentrations increased at around 09:00, suggesting an onset of NPF after the sunrise when the boundary layer begins to grow and turbulent mixing starts. On non-event days these particles showed the highest concentrations after the sunrise (06:00) and the sunset (18:00). The total particle concentration measured by the MAOS CPC showed a clear concentration increase on NPF event days, starting from 10:00, which clearly indicates that the particles had grown from smaller sizes into the 10 nm detection limit of the MAOS CPC. No clear diel pattern in the MAOS CPC measurements was visible on non-event days.

The type of NPF events that we observed are likely of regional nature, requiring relatively homogeneous air masses for at least a few hours (Vana et al., 2004; Manninen et al., 2010). The most likely explanations for why no new particle formation events were observed at the T0t site are: (i) either the lack of SO₂ sources for forming sulfuric acid or (ii) that the sampling at the less polluted T0t site was performed within the rainforest, where mixing with the atmospheric boundary layer above is hindered. The gaps, or fluctuations, in the usually distinct NPF shape in time-size-concentration plots could be caused by some degree of heterogeneity in the measured air masses. All NPF events occurred during the daytime, starting at around 08:00 - 09:00, 2 – 3 hours after sunrise. All NPF events took place during the wet season, which might be due to the lower condensation sink at this time of the year, as shown in Table 1. The median sulfuric acid concentrations, as measured by a quadrupole HOx CIMS (Martin et al, 2016, supplementary material), were about $9 \times 10^5 \text{ cm}^{-3}$ for both NPF event and non-event days. Similar sulfuric acid concentrations were reported for the Finnish boreal forest measurements in autumn, where about 12% of the days were classified as NPF event days (Kontkanen et al., 2017).

Back trajectories using HYSPLIT (<http://ready.arl.noaa.gov/hypub-bin/trajtype.pl?runtype=archive>; Rolph et al., 2017) were calculated using Global Data Assimilation System model data produced by the National Centers for Environmental Prediction (NCEP), and showed a clear difference in the air

mass origins arriving at the measurement site during the NPF event and non-event days. The back trajectories were calculated as ensembles for 24 hours to arrive at 13:00 UTC (09:00 local time) at 500m a. s. l. The back-trajectories were calculated on NPF event days and for each day prior to and following an NPF event day. If an NPF event occurred on two consecutive days, the day after both events was used for the non-event day back-trajectory calculations. On non-event days, the 50th percentile of air masses originated from 2. 9°S, 58.6°W and 545 m.a.s.l., a location upstream of the Amazon river. On NPF event days, the back-trajectory calculations show an origin at 2.5°S, 58.5°W and 602.5 m a. s. l.; further north, which is an area with dense rainforest. The results of the back-trajectory calculations are shown in Figure 10.

Figure 11 shows an example of an NPF event observed at the pasture site (T3), displaying MAOS SMPS data, NAIS total particle concentrations, and NAIS negative ion concentrations. The intermediate ion concentrations increased during this NPF event, starting at 08:00, with a continuous growth, reaching the smallest size channel of the MAOS SMPS at 10:00 (blue dashed line in panel d) of Figure 11). The same can be observed in the large particle and ion (4-12 nm) channel from the NAIS (red and black lines respectively).

Table 3 shows a comparison of the median particle and ion concentrations (25th – 75th percentiles in brackets), as well as the condensation sink, for the time window 08:00-12:00 comparing the NPF event and non-event days. The condensation sink was clearly lower on NPF event days (0.0018 s^{-1}) than on non-event days (0.003 s^{-1}), and the median concentration of intermediate (2-4 nm) ions and neutral particles was 1.3 times higher on NPF event days. The ion concentrations in the large size range were about a factor of 1.7 higher and neutral particle concentrations in the same size range were 2.4 times higher during the time of NPF compared to non-event days.

We also compared environmental variables, including the temperature, relative humidity and wind direction. No precipitation during any of the classified NPF events was observed, but on two classified NPF event days, precipitation periods were observed before or after the NPF events (starting at 06:00 and 17:00 respectively). The median temperature and RH were about the same for NPF event and non-event days, whereas the median wind direction changed (83°N on event days and 105.5°N during non-event days), consistent with the results from the back-trajectory analysis.

Table 4 shows the calculated growth rates, particle formation rates, and condensation sinks for each classified NPF event day. Note that here, the condensation sink was calculated for the time of the event, whereas the numbers in Tables 2 and 3 are for the whole day. The quantiles of both particle formation rate and growth rate were determined for two different size ranges (2-3 nm and 3-7 nm), and calculated separately for the ion and particle data. The results show considerably lower ion formation rates compared with neutral particle formation rates, consistent with observations made at most other continental sites (Manninen et al., 2010; Hirsikko et al., 2011). The growth rates of particles and ions were comparable to each other and typically smaller for the 2-3 nm size range than the 3-7 nm size range. An increase in the particle and ion growth rate with an increasing particle size has previously been reported at a few other sites (see Häkkinen et al., 2013, and references

523 therein). We observed two regimes when looking at the neutral 3-7 nm growth rate. On 3 days, the
524 growth rate was about 2 nm h^{-1} , with sulfuric acid concentrations of about $2 \times 10^6 \text{ cm}^{-3}$. According to
525 theoretical calculations about 10^7 cm^{-3} of sulfuric acid molecules can account for 1 nm h^{-1} (Nieminen
526 et al., 2010). It is most likely that other compounds are contributing to the growth. Other NPF event
527 days showed growth rates of about 14 nm h^{-1} for the same 3-7 nm size range, and the sulfuric acid
528 concentration was even lower (about $6 \times 10^5 \text{ cm}^{-3}$). These growth rates are most likely driven by
529 organic compounds (Tröstl et al., 2016). Tröstl et al. (2016) calculated that about 10^6 - 10^7 cm^{-3} of
530 highly oxidized organic compounds are required to explain a growth rate of about 10 nm h^{-1} .

531 4 Summary and Conclusions

532
533 We performed direct measurements of atmospheric new particle formation (NPF) events in the
534 Amazon region with state-of-the-art aerosol instrumentation. The measurement campaigns were
535 performed at two observation sites (T0t and T3) in the vicinity of Manaus in Brazil. One site was
536 located within the rainforest (T0t), providing long-term (September 2011 to January 2014)
537 measurement data, to complement data from a pasture site (T3, January to October 2014).
538

539 No NPF events were observed at the T0t site during the long-term measurement period. However,
540 we observed rain-induced ion and particle burst events ("rain-events") inside the rainforest during
541 264 of the 384 days. Concentrations of 2 - 4 nm and 4 - 12 nm ions and total particles were enhanced
542 by up to 3 orders of magnitude during such rain-events ($\sim 10^4$ - 10^5 cm^{-3}) at T0t site. The rain-events
543 occurred throughout the year, but the number of days with precipitation was the highest from
544 December to June corresponding to the wet season. Multiple rain-events could occur during the
545 same day, totaling 1491 rain-events in 643 rainy days for both sites together. The duration of the
546 rain-events ranged from a couple of minutes to 22 hours, but over 50% of the events lasted for <2
547 hours. During the rain-events, 0.8 - 2 nm and 2 - 4 nm negative ions increased more than the same-
548 size positive ions. The production of small (0.8 - 2 nm) and intermediate negative ions (2 - 4 nm)
549 during rain-events reached a maximum of 10^5 cm^{-3} at the T0t site.
550

551 At the pasture site, we observed a clear diel pattern in the cluster ion concentration during both the
552 wet and the dry season, with higher concentrations observed during the morning and evening. The
553 PSM observations showed a similar diel cycle for particles >1.5 nm, with higher concentrations in
554 the early morning, a dip in the afternoon, and an increase again in the evening after sunset. The diel
555 cycle was less pronounced inside the rainforest, indicating that the rainforest canopy hinders
556 vertical mixing.
557

558 We observed eight NPF events showing particle growth at the pasture site during January to March
559 2014. The formation rates were considerably higher for neutral particles than ions during these NPF
560 events. The growth rates of newly-formed ions and particles were comparable to each other and
561 showed a clear increase with increasing size in the sub-20 nm size range. We found two different
562 regimes for growth rates in the 3-7 nm size range; 3 out of 8 NPF days showed a growth rate of

about 2 nmh⁻¹, and on 4 out of 8 NPF days, a growth rate of about 14 nmh⁻¹ was observed. The sulfuric acid concentrations were similar for both NPF event and non-event days (approx. 9x10⁵ cm⁻³). Most likely the observed growth for all NPF events is driven by highly oxidized organic compounds (Tröstl et al., 2016).

The back-trajectory calculations using HYSPLIT did not show any clear difference between the days with high and low growth rates. Nevertheless, there was a clear difference in air mass origin between the days with NPF events when back-trajectories originated from the rainforest, and non-event days when back-trajectories originated from the Amazon river. As observed in SMPS measurements, particles grew to the sizes of around 60 nm during all the NPF events, above which they are able to act as cloud condensation nuclei (McFiggans et al, 2006; Andreae and Rosenfeld, 2008; Kerminen et al. 2012). There were clear differences in the median cluster and intermediate ion concentrations between the NPF event and non-event days for the local time window of 08:00-12:00. For NPF event days, the median intermediate ion and particle concentration was higher by a factor of 1.3 compared to non-event days. The condensation sink was also lower on the NPF event days (0.0016 s⁻¹) than on non-event days (0.003 s⁻¹). There were no NPF events observed during the dry season, when it is likely that the condensation sink is too high for new particle formation.

Acknowledgements

We acknowledge the Academy of Finland Centre of Excellence program (grant no. 272041). We acknowledge the Atmospheric Radiation Measurement (ARM) Climate Research Facility, a user facility of the United States Department of Energy, Office of Science, sponsored by the Office of Biological and Environmental Research, and support from the Atmospheric System Research (ASR) program of that office. D.W. wishes to acknowledge the Austrian Science Fund (FWF, grant no J-3951). P Artaxo acknowledges FAPESP project 2013/05014-0 and CNPq for funding. We thank field support from Alcides Ribeiro, Bruno Takeshi and Fabio Jorge. We acknowledge logistical support from the LBA Central Office, at the INPA – Instituto Nacional de Pesquisas da Amazonia.

References

- Aalto, P., Hämeri, K., Becker, E., Weber, R., Salm, J., Mäkelä, J. M., Hoell, C., O'Dowd, C. D., Karlsson, H., Hansson, H. C., Väkevä, M., Koponen, I. K., Buzorius, G., and Kulmala, M., Physical characterization of aerosol particles during nucleation events, *Tellus B*, 53:4, 344-358, 2001, doi: 10.1034/j.1600-0889.2001.530403.x.
- Andreae, M. O.: Aerosols before pollution, *Science*, 315, 50–51, 2007.

600

601 Andreae, M. O., and Rosenfeld, D.: Aerosol-cloud-precipitation interactions. Part 1. The nature and
602 sources of cloud-active aerosols, *Earth-Sci. Rev.*, 89, 13-41, 2008, Doi:
603 10.1016/j.earscirev.2008.03.001.

604

605 Andreae, M. O., Acevedo, O. C., Araùjo, A., Artaxo, P., Barbosa, C. G. G., Barbosa, H. M. J., Brito,
606 J., Carbone, S., Chi, X., Cintra, B. B. L., da Silva, N. F., Dias, N. L., Dias- Júnior, C. Q., Ditas, F.,
607 Ditz, R., Godoi, A. F. L., Godoi, R. H. M., Heimann, M., Hoffmann, T., Kesselmeier, J., Könemann,
608 T., Krüger, M. L., Lavric, J. V., Manzi, A. O., Lopes, A. P., Martins, D. L., Mikhailov, E. F., Moran-
609 Zuloaga, D., Nelson, B. W., Nölscher, A. C., Santos Nogueira, D., Piedade, M. T. F., Pöhlker, C.,
610 Pöschl, U., Quesada, C. A., Rizzo, L. V., Ro, C.-U., Ruckteschler, N., Sá, L. D. A., de Oliveira Sá,
611 M., Sales, C. B., dos Santos, R. M. N., Saturno, J., Schöngart, J., Sörgel, M., de Souza, C. M., de
612 Souza, R. A. F., Su, H., Targhetta, N., Tóta, J., Trebs, I., Trumbore, S., van Eijck, A., Walter, D.,
613 Wang, Z., Weber, B., Williams, J., Winderlich, J., Wittmann, F., Wolff, S., and Yáñez-Serrano, A.
614 M.: The Amazon Tall Tower Observatory (ATTO): overview of pilot measurements on ecosystem
615 ecology, meteorology, trace gases, and aerosols, *Atmos. Chem. Phys.*, 15, 10723–10776, 2015,
616 doi:10.5194/acp-15- 10723-2015.

617

618 Artaxo, P., Rizzo, L. V., Brito, J. F., Barbosa, H. M. J., Arana, A., Sena, E. T., Cirino, G. G., Bastos,
619 W., Martin, S. T., and Andreae, M. O.: Atmospheric aerosols in Amazonia and land use change: from
620 natural biogenic to biomass burning conditions, *Faraday Discuss.*, 165, 203–235, 2013.

621

622 Asmi, E., Sipilä, M., Manninen, H. E., Vanhanen, J., Lehtipalo, K., Gagné, S., Neitola, K., Mirme,
623 A., Mirme, S., Tamm, E., Uin, J., Komsaare, K., Attoui, M., and Kulmala, M.: Results of the first air
624 ion spectrometer calibration and intercomparison workshop, *Atmos. Chem. Phys.*, 9, 141-154, 2009,
625 doi:10.5194/acp-9-141-2009.

626

627 Backman, J., Rizzo, L. V., Hakala, J., Nieminen, T., Manninen, H. E., Morais, F., Aalto, P. P., Siivola,
628 E., Carbone, S., Hillamo, R., Artaxo, P., Virkkula, A., Petäjä, T., and Kulmala, M.: On the diurnal
629 cycle of urban aerosols, black carbon and the occurrence of new particle formation events in
630 springtime São Paulo, Brazil, *Atmos. Chem. Phys.*, 12, 11733-11751, 2012, doi:10.5194/acp-12-
631 11733-2012.

632

633 Dunne, E., Gordon, H., Kürten, A., Almeida, J., Duplissy, J., Williamson, C., Ortega, I. K., Pringle,
634 J.K., Adamov, A., Baltensperger, U., Barmet, P., Benduhn, F., Bianchi, F., Breitenlechner, M.,
635 Clarke, A., Curtius, J., Dommen, J., Donahue, N. M., Ehrhart, S., Flagan, R. C., Franchin, A., Guida,
636 R., Hakala, J., Hansel, A., Heinritzi, M., Jokinen, T., Kangasluoma, J., Kirkby, J., Kulmala, M., Kupc,
637 A., Lawler, M. J., Lehtipalo, K., Makhmutov, V., Mann, G., Mathot, S., Merikanto, J., Miettinen, P.,
638 Nenes, A., Onnela, A., Rap, A., Reddington, C. L. S., Riccobono, F., Richards, N. D. A., Rissanen,
639 M. P., Rondo, L., Sarnela, N., Schobesberger, S., Sengupta, K., Simon, M., Sipilä, M., Smith, J. N.,
640 Stozkhov, Y., Tomé, A., Tröstl, J., Wagner, P. E., Wimmer, D., Winkler, P. M., Worsnop, D. R., and
641 Carslaw K. S., Global atmospheric particle formation from CERN CLOUD measurements, *Science*,
642 354: 6316, 2016.

643

644 Dos Santos, V. N., Herrmann, E., Manninen, H. E., Hussein, T., Hakala, J., Nieminen, T., Aalto, P.
 645 P., Merkel, M., Wiedensohler, A., Kulmala, M., Petäjä, T., and Hämeri, K., *Atmos. Chem. Phys.*, 15;
 646 23:13717-13737, 2015, doi: 10.5194/acp-15-13717-2015.

647

648 Häkkinen, S. A. K., Manninen, H. E., Yli-Juuti, T., Merikanto, J., Kajos, M. K., Nieminen, T.,
 649 D'Andrea, S. D., Asmi, A., Pierce, J. R., Kulmala, M. and Riipinen, I.: Semi-empirical
 650 parameterization of size-dependent atmospheric nanoparticle growth in continental environments,
 651 *Atmos. Chem. Phys.*, 13, 15: 7665-7682, 2013, doi: 10.5194/acp-13-7665-2013.

652

653 Harrison, R. G., and Carslaw, K. S., Ion-Aerosol-cloud processes in the lower atmosphere, *Rev.*
 654 *Geophys.*, 41, 3 / 1012, 2003, doi:10.1029/2002RG000114.

655

656 Hirsikko, A, Laakso, L, Horrak, U, Aalto, P. P., Kerminen, V.-M., and Kulmala, M., Annual and size
 657 dependent variation of growth rates and ion concentrations in boreal forest, *Bor. Environ. Res.*, 10,
 658 357-369, 2005.

659

660 Hirsikko, A., Bergman, T., Laakso, L., Dal Maso, M., Riipinen, I., Hörrak, U., and Kulmala, M.,
 661 Identification and classification of the formation of intermediate ions measured in boreal forest,
 662 *Atmos. Chem. Phys.*, 7, 201-210, 2007.

663

664 Hirsikko, A., Nieminen, T., Gagné, S., Lehtipalo, K., Manninen, H. E., Ehn, M., Hörrak, U.
 665 Kerminen, V-M., Laakso, L., McMurry, P. H., Mirme, A., Mirme, S., Petäjä, T., Tammet, H.,
 666 Vakkari, V., Vana, M., and Kulmala, M. Atmospheric ions and nucleation: a review of observations,
 667 *Atmos. Chem. Phys.*, 11, 767-798, 2011, doi: 10.5194/acp-11-767-2011.

668

668 Hoppel, W. A., Theory of the electrode effect, *J. Atmos. Terr. Phys.*, Vol. 22, 1967.

669

670 Hörrak, U., Salm, J., and Tammet, H., Bursts of intermediate ions in atmospheric air, *J. Geophys.*
 671 *Res.: Atmos.*, 103: 13909-13915, 1998, doi: 10.1029/97JD01570.

672

673 Hörrak, U., Tammet, H., Aalto, P. P., Vana, M., Hirsikko, A.,
 674 Laakso, L., and Kulmala, M.: Formation of charged particles
 675 associated with rainfall: atmospheric measurements and lab experiments,
 676 *Rep. Ser. Aerosol Sci.*, 80, 180–185, 2006.

677

678 Kalivitis, N., Stavroulas, I., Bougiatioti, A., Kouvarakis, G., Gagné, S., Manninen, H. E., Kulmala,
 679 M., and Mihalopoulos, N.: Night-time enhanced atmospheric ion concentrations in the marine
 680 boundary layer, *Atmos. Chem. Phys.*, 12, 3627-3638, 2012, doi:10.5194/acp-12-3627-2012.

681

682 Kangasluoma J., Kuang C., Wimmer D., Rissanen M. P., Lehtipalo K., Ehn M., Worsnop, D. R.,
683 Wang, J., Kulmala M., and Petäjä T., Sub-3nm particle size and composition dependent response of
684 a nano-CPC battery, *Atmos. Meas. Tech.*, 7, 689–700, 2014, doi:10.5194/amt-7-689-2014.

685
686 Kerminen, V-M, Paramonov, M., Anttila, T., Riipinen, I., Fountoukis, C, Korhonen, H., Asmi, E.,
687 Laakso, L., Lihaväinen, H., Swietlicki, E., Svenningsson, B., Asmi, A., Pandis, S. N, Kulmala, M.,
688 and Petäjä, T., Cloud condensation nuclei production associated with atmospheric nucleation: a
689 synthesis based on existing literature and new results, *Atmos. Chem. Phys.*, 12, 24: 12037-12059,
690 2012, doi: 10.5194/acp-12-12037-2012.

691
692 Kontkanen, J., Lehtipalo, K., Ahonen, L., Kangasluoma, J., Manninen, H. E., Hakala, J., Rose, C.,
693 Sellegri, K., Xiao, S., Wang, L., Qi, X., Nie, W., Ding, A., Yu, H., Lee, S., Kerminen, V.-M., Petäjä,
694 T., and Kulmala, M., Measurements of sub-3 nm particles using a particle size magnifier in different
695 environments: from clean mountain top to polluted megacities, *Atmos. Chem. Phys.*, 2163–2187,
696 2017, doi:10.5194/acp-17-2163-2017.

697 Kulmala, M., Vehkämäki, H, Petäjä, T., Dal Maso, M., Lauri, A, Kerminen, VM, Birmili, and
698 McMurry, PH., Formation and growth rates of ultrafine atmospheric particles: a review of
699 observations, *J. Aerosol Sci.*, 35,143-176, 2004.

700
701 Kulmala, M., Petäjä, T., Nieminen, T., Sipilä, M., Manninen, H. E., Lehtipalo, K., Dal Maso, M.,
702 Aalto, P. P., Junninen, H., Paasonen, P., Riipinen, I., Lehtinen, K. E. J., Laaksonen, A., and Kerminen,
703 V.-M.: Measurement of the nucleation of atmospheric aerosol particles, *Nat. Protoc.*, 7, 1651–1667,
704 2012.

705
706 Kulmala, M., Kontkanen, J., Junninen, H., Lehtipalo, K., Manninen, HE, Nieminen, T., Petäjä, T.,
707 Sipilä, M., Schobesberger, S., Rantala, P., Franchin, A, Jokinen, T., Järvinen, E., Äijälä, M.,
708 Kangasluoma, J., Hakala, J., Aalto, P. P., Paasonen, P., Mikkilä, J., Vanhanen, J., Aalto, J., Hakola,
709 H., Makkonen, U., Ruuskanen, T., Mauldin, R. L., III, Duplissy, J., Vehkämäki, H., Back, J.,
710 Kortelainen, A., Riipinen, I., Kurten, T., Johnston, M. V., Smith, J. N. Ehn, M., Mentel, T. F.,
711 Lehtinen, K. E. J., Laaksonen, A., Kerminen, V.-M., and Worsnop, D. R., Direct Observations of
712 Atmospheric Aerosol Nucleation, *Science*, 339, 943, 2013.

713
714 Kulmala, M., Petäjä, T. Ehn, M., Thornton, J., Sipilä, M., Worsnop, D. R., and Kerminen, V. -M.,
715 Chemistry of Atmospheric Nucleation: On the Recent Advances on Precursor Characterization and
716 Atmospheric Cluster Composition in Connection with Atmospheric New Particle Formation, *Annu.*
717 *Rev. Phys. Chem.*, 65, 21–37, 2014.

718
719 Kulmala, M., Luoma, K., Virkkula, A, Petäjä, T., Paasonen, P., Kerminen, V.-M. Nie, W., Qi, X.,
720 Shen, Y., Chi, X., and Ding, A., On the mode-segregated aerosol particle number concentration load:
721 contributions of primary and secondary particles in Hyytiälä and Nanjing
722 *Bor. Environ. Res.*, 21, 319-331, 2016.

723
724 Leino, K., Nieminen, T., Manninen, H. E., Petäjä, T., Kerminen, V.-M., and Kulmala, M.,
725 Intermediate ions as a strong indicator of new particle formation bursts in a boreal forest, *Bor.*
726 *Environ. Res.*, 21, 274-286, 2016.

727
728 Lelieveld J., Butler, T. M., Crowley, J. N., Dillon, T. J., Fischer, H., Ganzeveld, L., Harder, H.,
729 Lawrence, M. G., Martinez, M., Taraborrelli, D., and Williams, J., Atmospheric oxidation capacity
730 sustained by a tropical forest, *Nature* 452, 737-740, 2008.

731

732 Manninen, H. E., Nieminen, T., Asmi, E., Gagné, S., Häkkinen, S., Lehtipalo, K., Aalto, P., Vana,
733 M., Mirme, A., Mirme, S., Hörrak, U., Plass-Dülmer, C., Stange, G., Kiss, G., Hoffer, A., Törő, N.,
734 Moerman, M., Henzing, B., de Leeuw, G., Brinkenberg, M., Kouvarakis, G. N., Bougiatioti, A.,
735 Mihalopoulos, N., O'Dowd, C., Ceburnis, D., Arneth, A., Svenningsson, B., Swietlicki, E., Tarozzi,
736 L., Decesari, S., Facchini, M. C., Birmili, W., Sonntag, A., Wiedensohler, A., Boulon, J., Sellegri,
737 K., Laj, P., Gysel, M., Bukowiecki, N., Weingartner, E., Wehrle, G., Laaksonen, A., Hamed, A.,
738 Joutsensaari, J., Petäjä, T., Kerminen, V.-M., and Kulmala, M.: EUCAARI ion spectrometer
739 measurements at 12 European sites – analysis of new particle formation events, *Atmos. Chem. Phys.*,
740 10, 7907–7927, 2010, doi:10.5194/acp-10-7907-2010.

741

742 Manninen, H. E., Mirme, S., Mirme, A., Petäjä, T., and Kulmala, M.: How to reliably detect molecular
743 clusters and nucleation mode particles with Neutral cluster and Air Ion Spectrometer (NAIS), *Atmos.*
744 *Meas. Tech.*, 9, 3577–3605, 2016, doi:10.5194/amt-9-3577-2016.

745

746 Martin, S. T., Andreae, M. O., Artaxo, P., Baumgardner, D., Chen, Q., Goldstein, A. H., Guenther,
747 A., Heald, C. L., Mayol-Bracero, O. L., McMurry, P. H., Pauliquevis, T., Poeschl, U., Prather, K. A.,
748 Roberts, G. C., Saleska, S. R., Silva Dias, M. A., Spracklen, D. V., Swietlicki, E., and Trebs, I.,
749 Sources and properties of Amazonian aerosol particles, *Rev. Geophys.*, 48, RG2002, 2010a, doi:
750 10.1029/2008RG000280.

751

752 Martin, S. T., Andreae, M. O., Althausen, D., Artaxo, P., Baars, H., Borrmann, S., Chen, Q., Farmer,
753 D. K., Guenther, A., Gunther, S. S., Jimenez, J. L., Karl, T., Longo, K., Manzi, A.,
754 Müller, T., Pauliquevis, T., Petters, M. D., Prenni, A. J., Pöschl, U., Rizzo, L. V., Schneider, J., Smith,
755 J. N., Swietlicki, E., Tota, J., Wang, J., Wiedensohler, A., and Zorn, S. R.: An overview of the
756 Amazonian Aerosol Characterization Experiment 2008 (AMAZE-08), *Atmos. Chem. Phys.*, 10,
757 11415–11438, 2010b, doi:10.5194/acp-10-11415-2010.

758 Martin, S. T., Artaxo, P., Machado, L. A. T., Manzi, A. O., Souza, R. A. F., Schumacher, C., Wang,
759 J., Andreae, M. O., Barbosa, H. M. J., Fan, J., Fisch, G., Goldstein, A. H., Guenther, A., Jimenez, J.
760 L., Pöschl, U., Silva Dias, M. A., Smith, J. N., and Wendisch, M.: Introduction: Observations and
761 Modeling of the Green Ocean Amazon (GoAmazon2014/5), *Atmos. Chem. Phys.*, 16, 4785–4797,
762 2016, doi:10.5194/acp-16-4785-2016.

763

764 Martin, S. T., Artaxo P., Machado, L., Manzi, A. O., Souza, R. A. F., Schumacher, C., Wang, J.,
765 Biscaro, T., Brito, J., Calheiros, A., Jardine, K., Medeiros, A., Portela, B., de Sá, S. S., Adachi, K.,
766 Aiken, A. C., Albrecht, R., Alexander, L., Andreae, M. O., Barbosa, H. M. J., Buseck, P., Chand, D.,
767 Comstock, J. M., Day, D. A., Dubey, M., Fan, J., Fast, J., Fisch, G., Fortner, E., Giangrande, S.,
768 Gilles, M., Goldstein, A. H., Guenther, A., Hubbe, J., Jensen, M., Jimenez, J. L., Keutsch, F. N., Kim,
769 S., Kuang, C., Laskin, A., McKinney, K., Mei, F., Miller, M., Nascimento, R., Pauliquevis, T.,
770 Pekour, M., Peres, J., Petäjä, T., Pöhlker, C., Pöschl, U., Rizzo, L., Schmid, B., Shilling, J. E., Silva
771 Dias, M. A., Smith, J. N., Tomlinson, J. M., Tóta, J., and Wendisch, M.: The Green Ocean Amazon
772 Experiment (GoAmazon2014/5) observes pollution affecting gases, aerosols, clouds and rainfall over
773 the rain forest, *Bull. Am. Meteor. Soc.*, 2017, doi:10.1175/BAMS-D-15-00221.1.

774

775 Mather, J. H., and Voyles, J. W.: The ARM Climate Research Facility: A review of structure and
776 capabilities, *Bull. Am. Meteor. Soc.*, 94, 377–392, 2013.

777

778 McFiggans, G, Artaxo, P., Baltensperger, U., Coe, H., Facchini, M. C., Feingold, G., Fuzzi, S., Gysel,
779 M., Laaksonen, A., Lohmann, U., Mentel, T. F., Murphy, D. M., O'Dowd, C. D., Snider, J. R.) and
780 Weingartner, E., The effect of physical and chemical aerosol properties on warm cloud droplet
781 activation, *Atmos. Chem. Phys.*, 6, 2593-2649, 2006.

782

783 Merikanto, J., Spracklen, D. V., Mann, G. W., Pickering, S. J., and Carslaw, K. S.: Impact of
784 nucleation on global CCN, *Atmos. Chem. Phys.*, 9, 8601-8616, 2009, doi:10.5194/acp-9-8601-2009.

785

786 Nieminen, T., Yli-Juuti, T., Manninen, H. E., Petäjä, T., Kerminen, V.-M., and Kulmala, M.:
787 Technical note: New particle formation event forecasts during PEGASOS–Zeppelin Northern
788 mission 2013 in Hyytiälä, Finland, *Atmos. Chem. Phys.*, 15, 12385-12396, 2015, doi:10.5194/acp-
789 15-12385-2015.

790

791 Nieminen, T., Lehtinen, K. E. J., and Kulmala, M., Sub-10 nm particle growth by vapor condensation
792 - effects of vapor molecule size and particle thermal speed, *Atmos. Chem. Phys.*, 10, 9773-9779,
793 2010, DOI: 10.5194/acp-10-9773-2010.

794

795 Rose, C., Sellegri, K., Velarde, F., Moreno, I., Ramonet, M., Weinhold, K., Krejci, R. Ginot, P.,
796 Andrade, M., Wiedensohler, A., and Laj, P., Frequent nucleation events at the high altitude station of
797 Chacaltaya (5240 m a.s.l.), Bolivia, *Atmos. Environ.*, 102, 18-29, DOI:
798 10.1016/j.atmosenv.2014.11.015, 2015.

799 Rolph, G., A. Stein and B. Stunder, Real-time Environmental Applications and Display sYstem:
800 READY, *Environmental Modelling & Software*, 95, 210-228, 2017,
801 doi:10.1016/j.envsoft.2017.06.025.
802

803 Tammet, H., Hörrak, U., and Kulmala, M.: Negatively charged nanoparticles produced by splashing
804 of water, *Atmos. Chem. Phys.*, 9, 357-367, 2009, doi:10.5194/acp-9-357-2009.

805

806 Tröstl, J., Chuang, W. K., Gordon, H., Heinritzi, M., Yan, C., Molteni, U., Ahlm, L., Frege, C.,
807 Bianchi, F., Wagner, R., Simon, M., Lehtipalo, K., Williamson, C., Craven, J. S., Duplissy, J.,
808 Adamov, A., Almeida, J., Bernhammer, A.-K., Breitenlechner, M., Brilke, S., Dias, A., Ehrhart, S.,
809 Flagan, R. C., Franchin, A., Fuchs, C., Guida, R., Gysel, M., Hansel, A., Hoyle, C. R., Jokinen, T.,
810 Junninen, H., Kangasluoma, J., Keskinen, H., Kim, J., Krapf, M., Kürten, A., Laaksonen, A., Lawler,
811 M., Leiminger, M., Mathot, S., Möhler, O., Nieminen, T., Onnela, A., Petäjä, T., Piel, F. – M.,
812 Miettinen, P., Rissanen, M. P., Rondo, L., Sarnela, N., Schobesberger, S., Sengupta, K., Sipilä, M.,
813 Smith, J. N., Steiner, G., Tomè, A., Virtanen, A., Wagner, A.C., Weingartner, E., Wimmer, D.,
814 Winkler, P. M., Ye, P., Carslaw, K. S., Curtius, J., Dommen, J., Kirkby, J., Kulmala, M., Riipinen,
815 I., Worsnop, D.R., Donahue, N. M. and Baltensperger, U., The role of low-volatility organic

816 compounds in initial particle growth in the atmosphere, *Nature*, 533, 527-531, 2016,
817 doi:10.1038/nature18271.

818

819 Vanhanen, J., Mikkilä, J., Lehtipalo, K., Sipilä, M., Manninen, H. E., Siivola, E., Petäjä, T., and
820 Kulmala, M.: Particle size magnifier for nano-CN detection. *Aerosol Sci. Technol.*, 45:533–542,
821 2011.

822

823 Suni, T., Kulmala, M., Hirsikko, A., Bergman, T., Laakso, L., Aalto, P. P., Leuning, R., Cleugh, H.,
824 Zegelin, S., Hughes, D., van Gorsel, E., Kitchen, M., Vana, M., Hörrak, U., Mirme, S., Mirme, A.,
825 Sevanto, S., Twining, J., and Tardos, C.: Formation and characteristics of ions and charged aerosol
826 particles in a native Australian Eucalypt forest, *Atmos. Chem. Phys.*, 8, 129-139, 2008,
827 doi:10.5194/acp-8-129-2008.

828

829 Svenningsson, B., Arneth, A., Hayward, S., Holst, T., Massling, A., Swietlicki, E., Hirsikko, A.,
830 Junninen, H., Riipinen, I., Vana, M., Dal Maso, M., Hussein, T., and Kulmala, M.: Aerosol particle
831 formation events and analysis of high growth rates observed above a subarctic wetland-forest mosaic,
832 *TellusB*, 60B, 353–364, 2008.

833

834 Vana, M., Kulmala, M., Dal Maso, M. and Hörrak, U., Comparative study of nucleation mode aerosol
835 particles and intermediate air ions formation events at three sites, *J. Geophys. Res.*, VOL. 109,
836 D17201, 2004, doi:10.1029/2003JD004413.

837

838 Vana, M., Ehn, M., Petäjä, T., Vuollekoski, H., Aalto, P., de Leeuw, G., Ceburnis, D., O'Dowd, C.
839 D., and Kulmala, M. Characteristic features of air ions at Mace Head on the west coast of Ireland,
840 *Atmos. Res.*, 90, 278-286, 2008, DOI: 10.1016/j.atmosres.2008.04.007.

841

842 Vanhanen, J., Mikkilä, J., Lehtipalo, K., Sipilä, M., Manninen, H. E., Siivola, E., Petäjä, T. and
843 Kulmala, M. (2011), Particle Size Magnifier for Nano-CN Detection, *Aerosol Sci. Technol.*, 45: 4,
844 533 — 542, 2011, DOI: 10.1080/02786826.2010.547889.

845

846 Wagner, R., Manninen, H. E., Franchin, A., Lehtipalo, K., Mirme, S., Steiner, G., Petäjä, T., and
847 Kulmala, M.: On the accuracy of ion measurements using a Neutral cluster and Air Ion Spectrometer,
848 *Bor. Environ. Res.*, 21, 230-241, 2016.

849

850 Wang, J., Krejci, R., Giangrande, S., Kuang, C., Barbosa, H. M. J., Brito, J., Carbone, S., Chi, X.,
851 Comstock, J., Ditas, F., Lavric, J., Manninen, H. E., Mei, F., Moran-Zuloaga, D., Pöhlker, C., Pöhlker,
852 M. L., Saturno, J., Schmid, B., Souza, R. A. F., Springston, S. R., Tomlinson, J. M., Toto, T., Walter,
853 D., Wimmer, D., Smith, J. N., Kulmala, M., Machado, L.A. T., Artaxo, P., Andreae, M. O., Petäjä,
854 T., and Martin, S. T., Amazon boundary layer aerosol concentration sustained by vertical transport
855 during rainfall, *Nature*, 2016, doi:10.1038/nature19819.

856

857 Wang, M., and Penner, J. E., Aerosol indirect forcing in a global model with particle nucleation,
858 *Atmos. Chem. Phys.*, 9:1, 239-260, 2009.

859

860 Yu, F., and Luo, G.: Simulation of particle size distribution with a global aerosol model: contribution
861 of nucleation to aerosol and CCN number concentrations, *Atmos. Chem. Phys.*, 9: 20, 7691-7710,
862 2009.

863

864 Zhou, J., Swietlicki, E., Hansson, H. C. and Artaxo, P.: Submicrometer aerosol particle size
865 distribution and hygroscopic growth measured in the Amazon rain forest during the wet season, J.
866 Geophys. Res. D Atmos., 107(20), doi:10.1029/2000JD000203, 2002.

890 **Tables**

891 Table 1. Overall data availability for the measurements presented in the manuscript.

		# of days with rain data	# of days with rain event	NAIS particle data	NAIS ion data	NPF
2011	August	5	2	0	0	0
	September	6	1	4	4	0
	October	28	14	31	31	0
	November	30	18	30	30	0
	December	31	23	16	16	0
total 2011		100	58	81	81	0
2012	January	31	31	31	31	0
	February	29	18	29	29	0
	March	31	0	9	9	0
	April	30	29	29	29	0
	May	31	25	16	16	0
	June	30	23	4	4	0
	July	31	24	0	0	0
	August	31	12	0	0	0
	September	30	4	0	0	0
	October	31	0	0	0	0
	November	30	5	0	0	0
	December	31	24	16	16	0
total 2012		366	195	134	134	0
2013	January	31	26	31	31	0
	February	28	28	28	28	0
	March	31	24	31	31	0
	April	30	29	30	30	0
	May	31	27	31	31	0
	June	30	23	30	30	0
	July	31	9	31	31	0
	August	31	15	26	26	0
	September	30	13	30	30	0
	October	30	16	31	31	0
	November	30	24	30	30	0
	December	31	17	31	31	0
total 2013		364	251	360	360	0
2014	January T0t (rain data only from T0t)	20	13	25	25	0
	January T3	0	0	5	5	2
	February	28	23	28	28	2
	March	31	28	31	31	4
	April	30	27	23	23	0
	May	0	0	0	0	0
	June	0	0	0	0	0
	July	0	0	0	0	0

		# of days with rain data	# of days with rain event	NAIS particle data	NAIS ion data	NPF
	August	31	13	6	6	0
	September	30	16	30	12	0
	October	31	19	13	13	0
total 2014		201	139	161	143	8
total		1031	643	736	718	8

Table 2. A comparison of the two measurement sites and the wet and the dry season. The values from the pasture site are on the left-hand side, the values from the inside the rainforest site on the right-hand side. The months for the wet season are January to June and July to December for both measurement sites. Aerosol and ion parameters from the NAIS measurements listed are: the ion concentrations in three size bins (0.8-2, 2 - 4 and 4 - 12 nm); the neutral particle concentrations in two different size bins from the NAIS (2 - 4 and 4 -12 nm), and the total particle concentrations (>10 nm) from the MAO CPC measurements and the calculated condensation sink values from the SMPS are also shown. The numbers present median values and the 25th-75th percentiles are in the brackets. The environmental parameters shown are the temperature, the relative humidity, the precipitation rate, the wind direction and the wind speed.

936
937

	Pasture site (T3)		Inside rainforest (T0t)	
Particle and ion concentrations				
Season	Wet	Dry	Wet	Dry
Cluster ions (0.8-2 nm) [cm ⁻³]	1300(-) (1000-1800)	890(-) (468-1400)	856 (-) (535 -1300) 549(+) (298 - 924)	952(-) (637- 1400) 537 (+) (297-915)
Intermediate ions (2-4 nm) [cm ⁻³]	6 (-) (4-11)	5(-) (1-10)	17(-) (10-28) 34(+) (20-48)	17 (-) (10-28) 34(+) (21-48)
Large ions (4-12 nm) [cm ⁻³]	20(-) (11-32)	12(-) (4 - 25)	8(-) (4-16) 8(+) (4-14)	8(-) (4-16) 8 (4-14)
Intermediate particles (2-4 nm) [cm ⁻³]	612 (304 - 1000)	640 (291 - 1200)	358 (128-713)	404 (155-819)
Large particles (4 - 12 nm) [cm ⁻³]	363 (196 - 675)	314 (179 - 551)	115 (42-250)	141(-) (52-313)
CPC total particles (>10 nm) [cm ⁻³]	928 (516 - 1500)	2000 (1100 - 3000)	-	-
SMPS condensation sink [s ⁻¹]	1.9x10 ⁻³ (9.5x10 ⁻⁴ -2.4x10 ⁻³)	5.2x10 ⁻³ (2.3x10 ⁻³ -6.1x10 ⁻³)	-	-
Environmental parameters				
Temp [°C]	26 (24.4 – 29.9)	25.9 (24.5 – 28.6)	24.1 (23.2 -25.6)	24.5 (23.4 - 26.5)
RH [%]	92.8 (76 – 97.3)	94.6 (83 - 98)	96.9 (93-98)	94.4 (87 - 97)
Total average precipitation [mm]	35.6	49	578	236
Wind direction [°; relative to north]	114.7 (32.7 – 231.5)	94.7 (45.8 – 178.6)	94 (58-138)	105 (58 - 167)
Wind speed [m s ⁻¹]	1.1 (0.5 – 2.1)	1.3 (0.6 – 2.4)	0.2 (0.2 – 0.3)	0.2 (0.2 – 0.3)

938
939
940
941

942 Table 3. The parameters from the pasture site for NPF days and non-event days are shown. The
 943 values shown are: the median total particle concentration measured by a CPC, the median neutral
 944 particle concentrations measured by the NAIS in two size ranges (2 - 4 and 4 - 12 nm), and the
 945 median negative ion concentrations from the NAIS in three size ranges (0.8-2, 2 - 4 and 4 – 12 nm).
 946 The values are calculated for the time window 08:00 – 12:00, which is when the NPF events take
 947 place. The numbers in the brackets represent the 25th and 75th percentiles. The second part of the
 948 table includes median numbers of environmental parameters for the whole day: temperature, RH,
 949 Precipitation and wind direction for NPF /non-event days.
 950

Particle and ion concentrations- 08:00 – 12:00 LT		
	NPF day	Non NPF day
Cluster ions (0.8-2 nm) [cm⁻³]	1000 (-) (862 - 1300)	1000 (-) (865 - 1300)
Intermediate ions (2-4 nm) [cm⁻³]	10 (-) (5 - 22)	8 (-) (4-15)
Large ions (4-12 nm) [cm⁻³]	29 (-) (17 - 56)	17 (-) (7 - 33)
Intermediate particles (2-4 nm) [cm⁻³]	800 (865 - 1300)	640 (281 - 1200)
Large particles (4-12 nm) [cm⁻³]	785 (446-1300)	321 (170 - 580)
CPC total particles (>10 nm) [cm⁻³]	1000 (607 - 1900)	938 (400 - 1800)
Full day data		
SMPS Condensation sink [s⁻¹]	1.8x10 ⁻³ (1x10 ⁻³ -2.8x10 ⁻³)	3.2x10 ⁻³ (1.7x10 ⁻³ -5.3x10 ⁻³)
Environmental parameters-full day		
	NPF day	Non NPF day
Temp [°C]	26.5 (24.8 – 31.9)	26 (24.4 – 29.2)
RH [%]	90.6 (66.6 – 96.3)	93.5 (78.9 – 97.6)
Precipitation rate [mm hr⁻¹]	0.16 (0.15 – 0.35)	0 (0 – 0.16)
Wind direction [°; relative to north]	83.8 (7.3 – 200.6)	104.2 (39.6 – 215.5)
Wind speed [m s⁻¹]	0.9 (0.23 – 1.8)	1.25 (0.6 – 2.3)

951
 952
 953

954 Table 4. The growth rates (GR, nmh⁻¹) and the nucleation rates (J; cm⁻³s⁻¹) determined from the NAIS
 955 ion and particle data for each nucleation event are presented. Both, the GR values and the
 956 nucleation rates present median values for positive and negative ions. Also, the median values for
 957 the calculated condensation sink values (CS; s⁻¹) for each event are shown. The condensation sink
 958 parameter is calculated from the SMPS size distributions. The last line of the table shows the median
 959 values for GR and J for all the nucleation event days are shown, except the ion GR at 2-3 nm of 19.8
 960 nmh⁻¹ on 06.02.2014 is considered to be an outlier and not included in the median.
 961

Size bins	2-3 nm				3-7 nm				
	<i>Particles</i>		<i>ions</i>		<i>Particles</i>		<i>Ions</i>		
	GR (nm h ⁻¹)	J (cm ⁻³ s ⁻¹)	GR (nm h ⁻¹)	J (cm ⁻³ s ⁻¹)	GR (nm h ⁻¹)	J (cm ⁻³ s ⁻¹)	GR (nm h ⁻¹)	J (cm ⁻³ s ⁻¹)	CS (s ⁻¹)
29.01.2014	0.8	0.19	1.4	0.003	2.8	0.097	1.7	0.001	-
30.01.2014	-	-	3.7	0.011	13.6	-	7.1	0.13	0.00076
06.02.2014	0.8	-	19.8	0.07	29	0.87	11	0.01	0.0016
12.02.2014	0.7	0.17	1.2	0.005	1.3	0.09	1.2	0.003	0.0016
12.03.2014	1.1	0.2	1.7	0.002	13.3	-	11.2	0.008	0.0014
13.03.2014	1.5	0.2	1.6	-	1.2	-	8	-	0.0015
18.03.2014	-	-	0.7	0.002	-	-	7.7	0.009	0.0017
25.03.2014	0.8	0.11	-	-	15.7	0.4	15.8	0.018	0.0017
median	0.8	0.18	1.6	0.004	13.3	0.25	7.85	0.009	0.0016

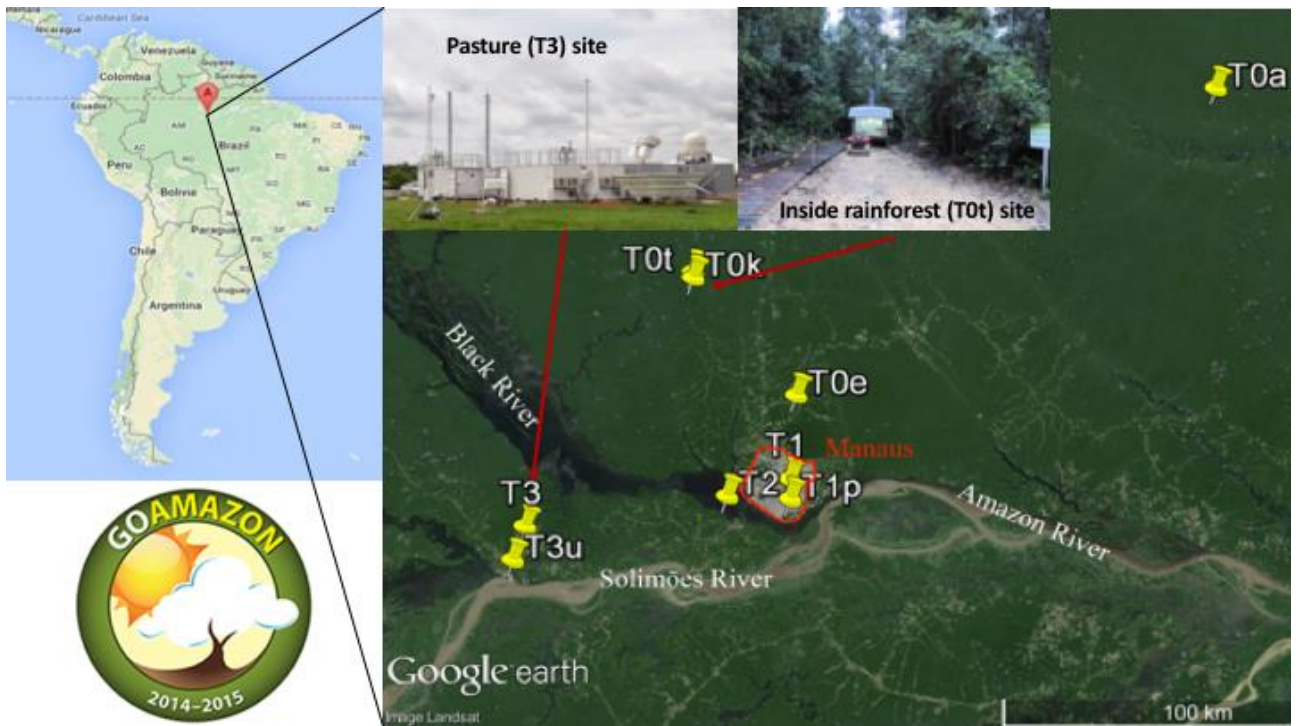


Figure 1. The location on the map and photos of the inside rainforest (T0t) and open pasture (T3) sampling sites in Amazonas is shown here. The left column shows a map of South America and the right-hand side shows a satellite view and photos of the T0t and T3 environment.

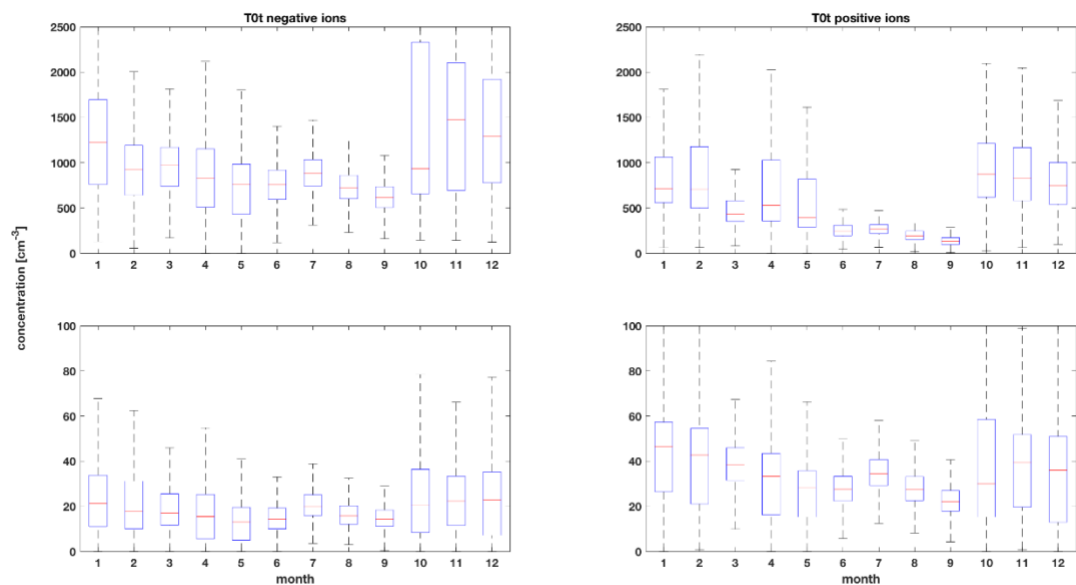
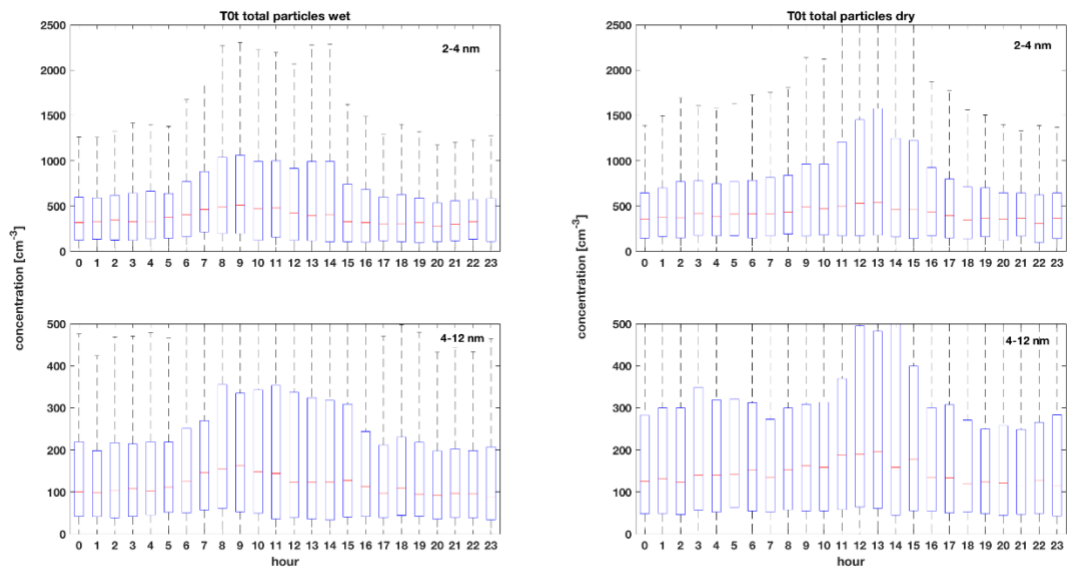


Figure 2. The median annual variations for positive and negative cluster (0.8 – 2nm) and intermediate (2 - 4 nm) ions, from the inside the rainforest site are shown. The boxes show the 25th-75th percentile and the whiskers are 1.5 x IQR (interquartile range), data points beyond the whiskers are considered outliers.



1011
 1012
 1013 Figure 3. The median diel patterns of the intermediate (2-4 nm) and the large (4-12 nm) particles
 1014 from the NAIS measurements at the T0t measurement site are shown. On the left -hand side are
 1015 the values for the wet and on the right-hand side the values for the dry season. The boxes represent
 1016 25th – 75th percentiles and the whiskers are 1.5 x IQR (interquartile range), data points beyond the
 1017 whiskers are considered outliers.
 1018

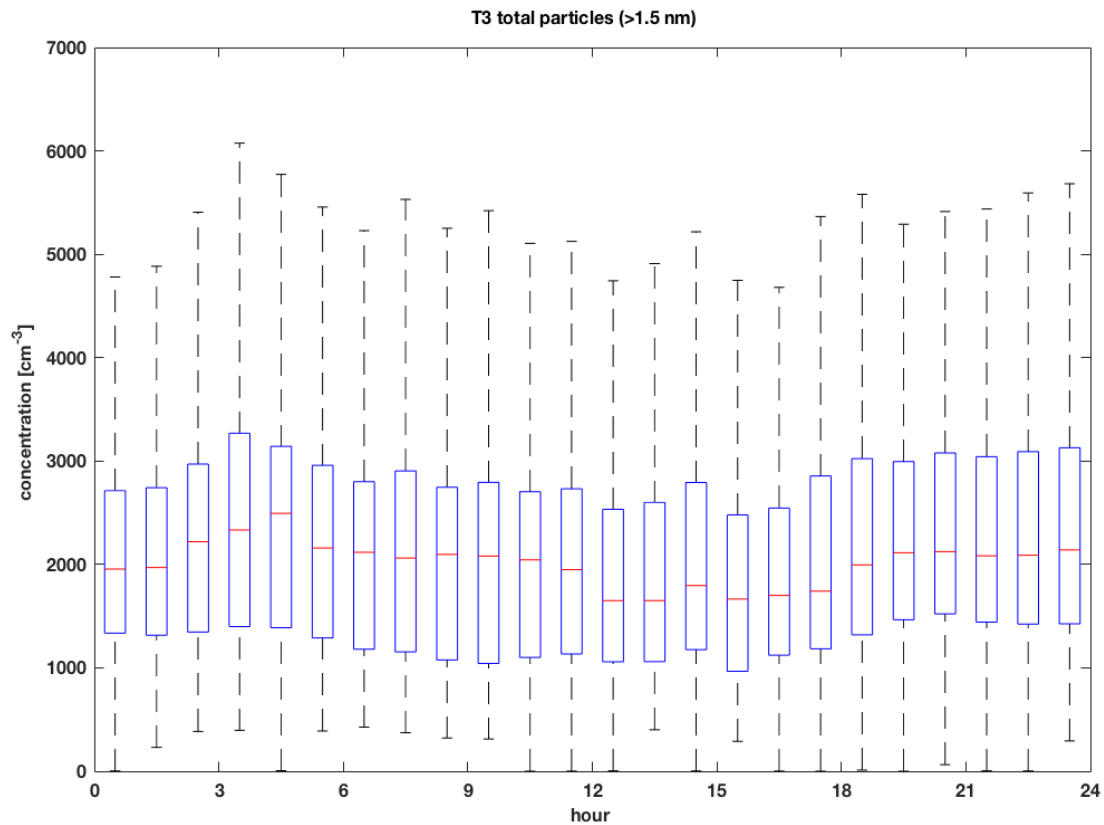
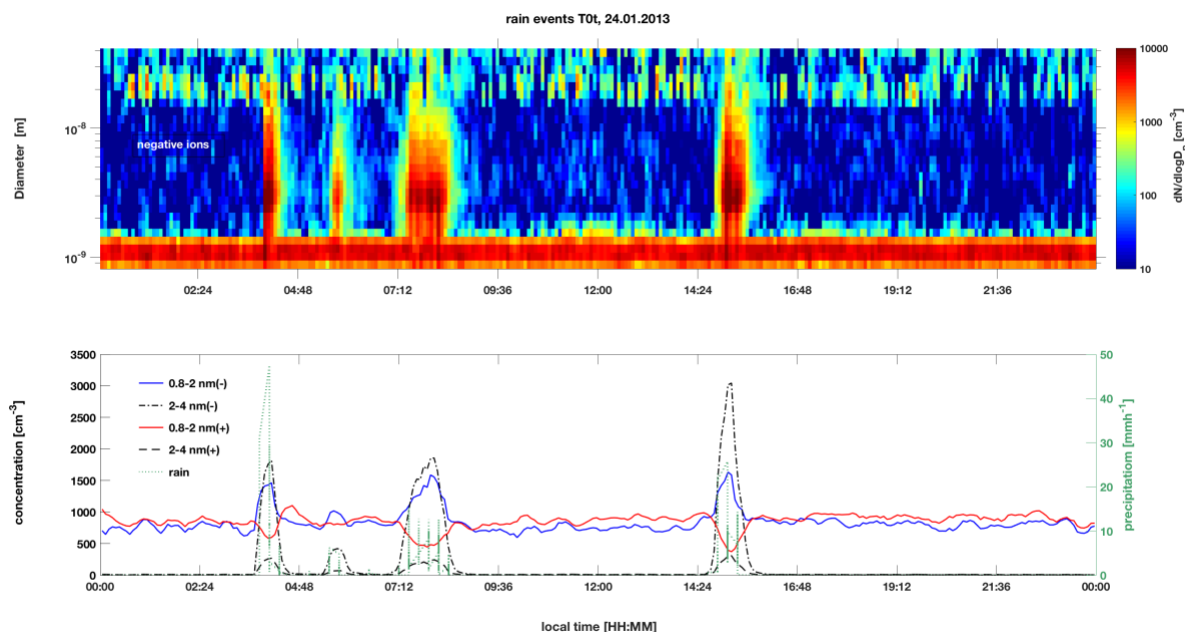
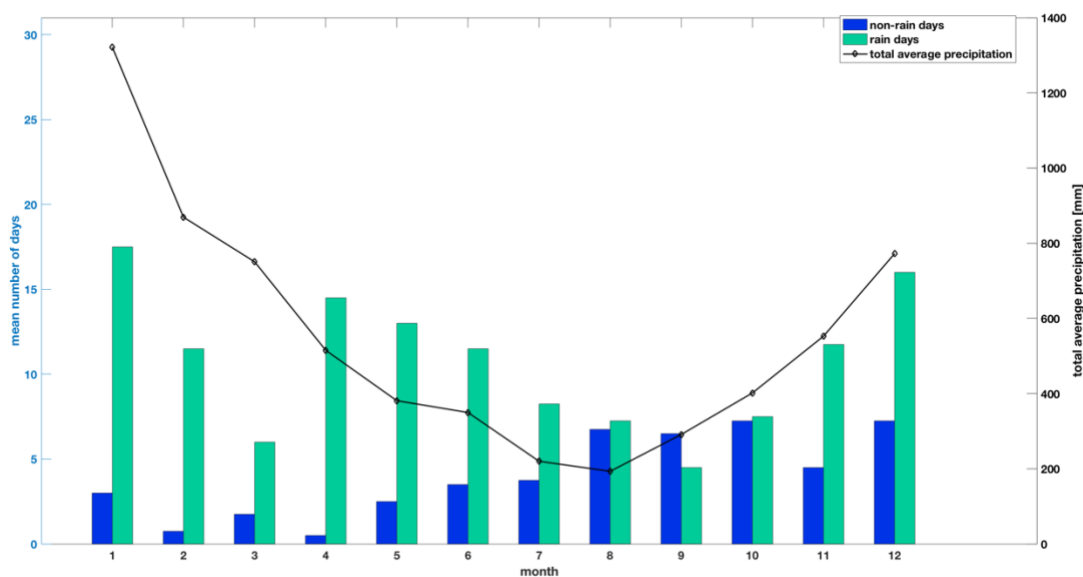


Figure 4. The diel cycle of particles bigger than 1.5 nm measured by the PSM during the dry season at the pasture site is shown. In total, 38 days of data were used. The data show hourly median concentrations, the boxes represent the 25th and 75th percentiles and the whiskers are 1.5 x IQR (interquartile range), data points beyond the whiskers are considered outliers.



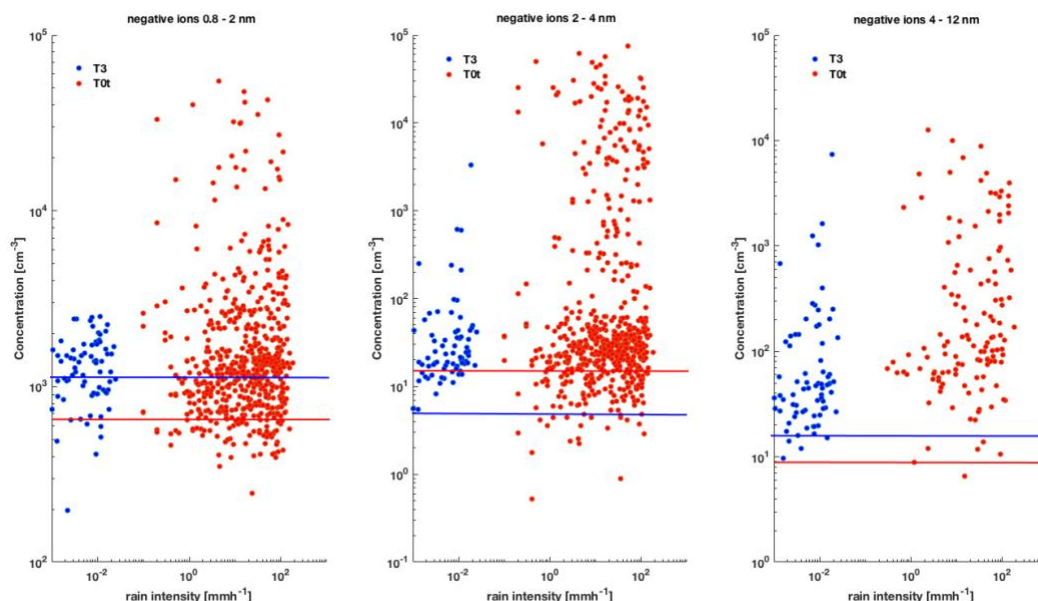
1035
1036

1037 Figure 5. An example for a rain event at the T0t, inside the rainforest measurement site is shown.
1038 The upper panel shows the surface Figure of the NAIS negative ion channel. The lower panel
1039 shows (i) the concentrations of positive (red line), (ii) negative (blue line) cluster ions (0.8 – 2 nm),
1040 (iv) positive (dashed black line), and (v) negative (dot-dashed line) intermediate (2 -4 nm) ions on
1041 the left - hand axis. The precipitation rate in mmh⁻¹ is shown in green on the right - hand axis.



1042
1043
1044
1045
1046
1047
1048
1049
1050

Figure 6. The statistics of the precipitation days at the T0t site are shown. The blue bars show the mean number of days per month with no precipitation and the green bars the mean number of days per month with precipitation rates above zero. The black line shows the average total precipitation per month in mm on the right-hand axis.



1051
1052
1053
1054
1055
1056
1057
1058
1059
1060
1061
1062

Figure 7. The maximum (99 percentile) negative ion concentrations as a function of rain intensity at the inside rainforest site (T0t) between September 2011 and January 2014 (red circles) are shown. For comparison, the ion concentrations from the open pasture site are added (blue circles). The lines indicate the median ion concentrations at the absence of precipitation for T0t (red) and T3 (blue).

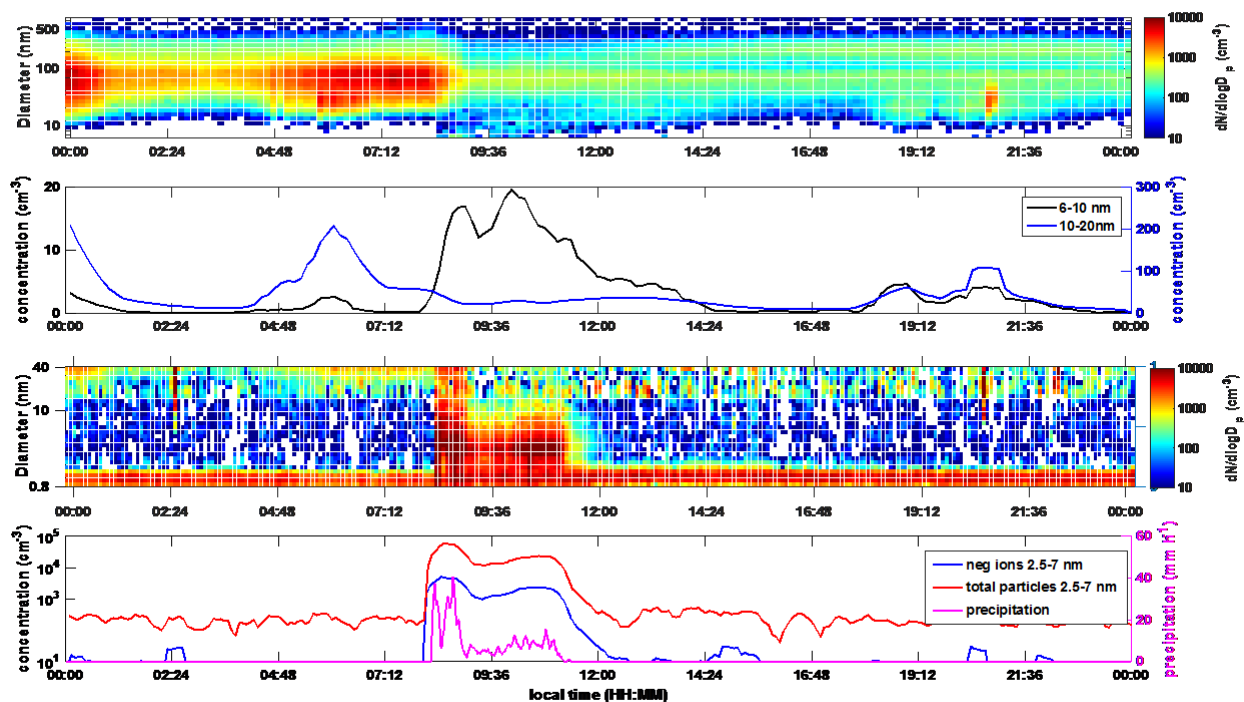


Figure 8. An Example for of a rain-induced event is shown. The upper panel shows the surface Figure for total particles (DMPS). The second panel from the top shows the particle concentrations measured by the DMPS for the size range of 6-10 nm (black line, left-hand axis) and the size range of 10-20 nm (blue line, right-hand axis). The third panel from the top shows the surface Figure for the negative ions, measured by the NAIS. The lower panel shows the negative ion concentrations for 2.5-7 nm in blue and the neutral particle concentration in the same size range from the NAIS in red. For the neutral particles, the scale is on the left-hand axis. The pink trace shows the precipitation rate in mm h^{-1} on the right-hand axis.

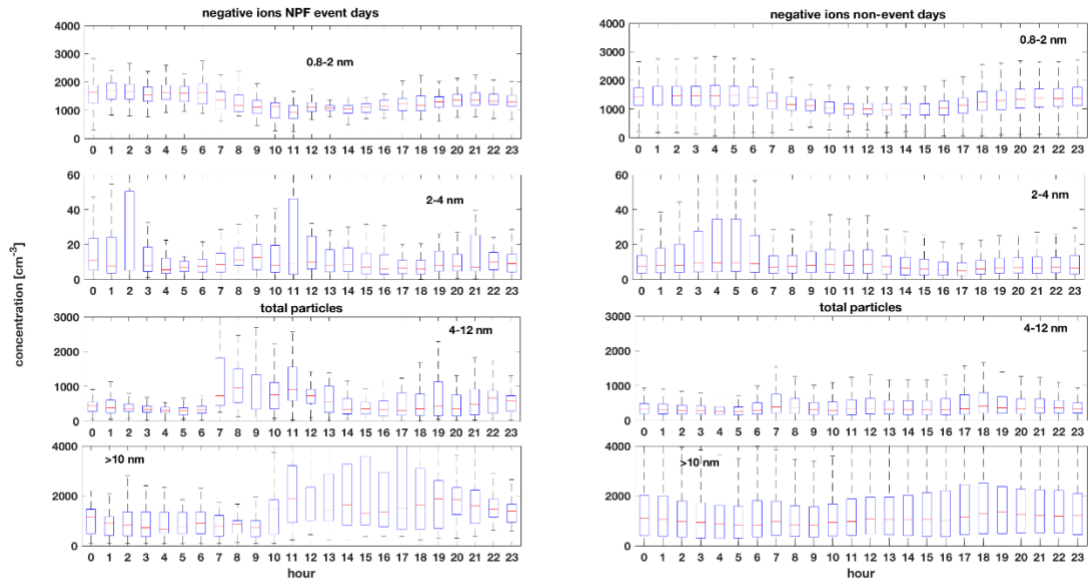


Figure 9. The median diel cycles of cluster ions (0.8 – 2nm), intermediate ions (2 – 4 nm), large (4 – 12 nm) neutral particles, and total particles (>10 nm) for new particle formation event days (left) and non-event days (right) are shown. The boxes show the 25th -75th percentiles and the whiskers are 1.5 x IQR (interquartile range), data points beyond the whiskers are considered outliers.

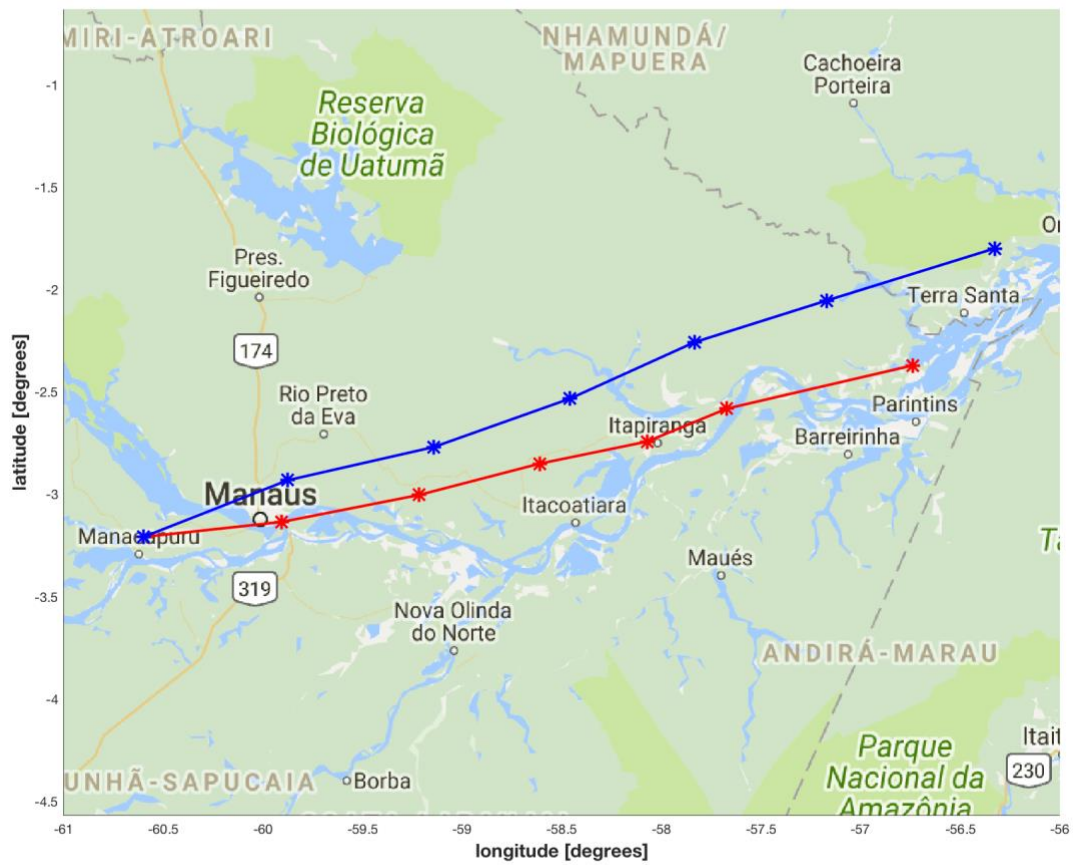
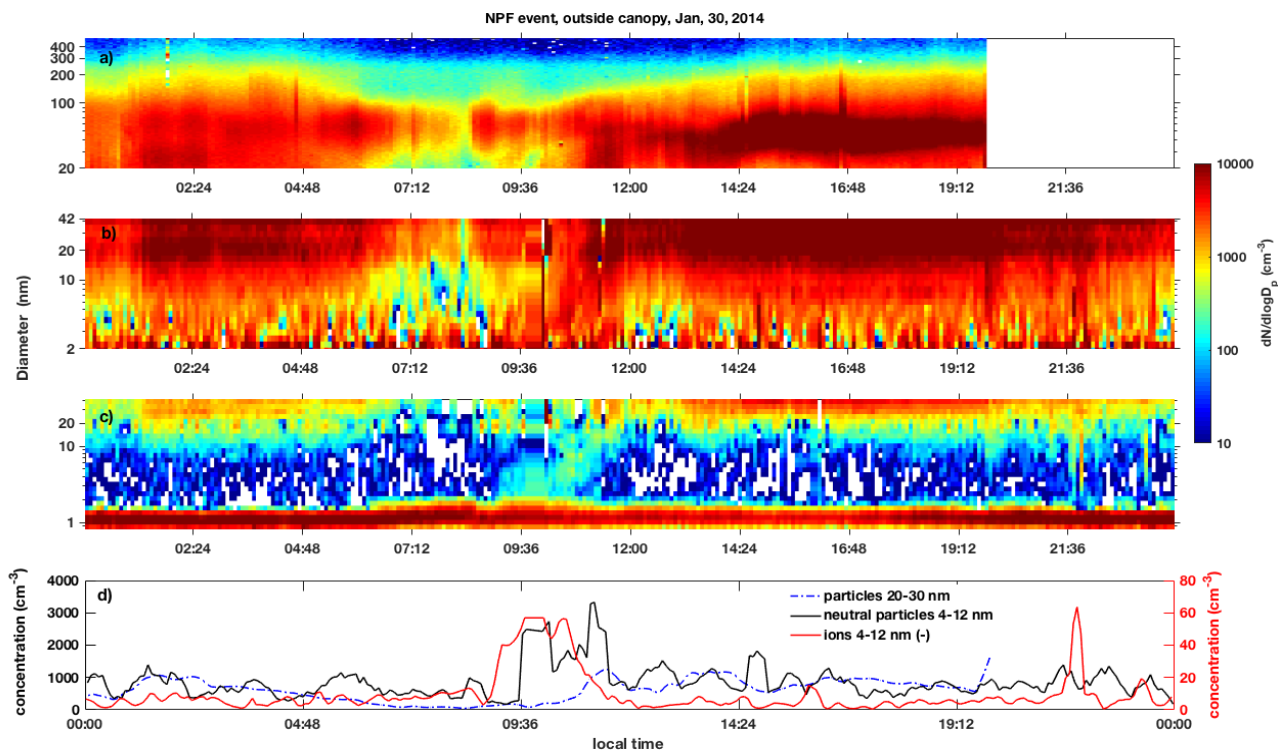


Figure 10. The median back trajectories for NPF (blue) and non-event (red) days are shown. The trajectories were calculated as ensembles, 24hours backwards arriving at 09:00 local time at 500 m a.s.l. at the open pasture measurement site.



1116
1117

1118 Figure 11. One example of an NPF event day, as observed at the open pasture (T3) site. (a) shows
1119 the surface Figure from the SMPS, (b) and (c) show the surface Figures from the NAIS, (b) for neutral
1120 particles and (c) for negative ions. The color code indicates the measured concentrations. Panel (d)
1121 shows concentrations for the 20-30nm size range from the SMPS on the left-hand axis (blue dashed
1122 line). The solid red line shows the 4-12 nm negative ion concentration on the right-hand axis and
1123 the solid black line the 4-12 nm neutral particle concentration on the left-hand axis.